Title
ELECTROSTATIC DEFLECTOR CALCULATIONS FOR THE BERKELEY 88-INCH CYCLOTRON

Authors
Garren, Alper A.
Judd, David L.
Smith, Lloyd
et al.

Publication Date
1962-05-15

UCRL 10067 Rev
cy 2.

University of California

Ernest O. Lawrence Radiation Laboratory

Berkeley, California

DISCLAIMER

For publication in Nuclear Instruments and Methods
(this replaces copy previously sent)

UCRL-10067 Rev

UNIVERSITY OF CALIFORNIA

Lawrence Radiation Laboratory
Berkeley, California

Contract No. W-7405-eng-48

ELECTROSTATIC DEFLECTOR CALCULATIONS FOR THE BERKELEY 88-INCH CYCLOTRON

Alper A. Garren, David L. Judd, Lloyd Smith,
and Hans A. Willax

May 15, 1962

ELECTROSTATIC DEFLECTOR CALCULATIONS FOR THE BERKELEY 88-INCH CYCLOTRON

Alper A. Garren, David L. Judd,
Lloyd Smith, and Hans A. Willax

Lawrence Radiation Laboratory
University of California
Berkeley, California

May 15, 1962

ABSTRACT

Early computer calculations showed that an electrostatic channel would have to be very narrow to cause sufficient deflection at high energy. One alternative considered was a system of three electrostatic channels in series, acting as a one-turn regenerative extractor. Such a system could easily achieve the required deflection, but at the expense of simplicity. A magnetic-channel to reinforce the electrostatic channel likewise appeared difficult for a variable-energy machine.

Detailed studies of a simple electrostatic channel began with development of an analytic-graphical method of calculating channel efficiency. By this method one can estimate acceptance as a function of radial turn separation, amplitude and frequency of radial oscillations, and channel geometry. A computer code was then developed to compute channel shapes and calculate acceptance more accurately by following the fate of a representative sample of orbits in the presence of the channel. Use of this code indicated that highest acceptance would be obtained if the channel entrance is set out at 39 in. provided the resonances at $\nu_r = 1$ and $\nu_r = 2\nu_z$ could be safely traversed, as was believed possible. Some calculations on transition through the $\nu_r = 2\nu_z$ resonance are presented.

ELECTROSTATIC DEFLECTOR CALCULATIONS FOR THE BERKELEY 88-INCH CYCLOTRON†

Alper A. Garren, David L. Judd, Lloyd Smith, and Hans A. Willax††

Lawrence Radiation Laboratory
University of California
Berkeley, California

May 15, 1962

1. Introduction

This paper presents an account of some of the calculations relating to the beam-extraction system for the Berkeley 88-inch cyclotron. We wished to design a system which could extract at least 10% of the internal beam, for the full range of particles and energies that this machine can accelerate.

The system chosen is a single conventional electrostatic (ES) channel. Various alternatives were considered with varying degrees of thoroughness, as follows:

(i) An ES channel with hot-glass electrodes, to permit higher electric fields. This system had not been proven feasible in a radiation environment.

(ii) Three ES channels in series. This system, discussed in Sec. 2 of this paper, seemed too complex.

(iii) A magnetic channel. This seemed too inflexible for a variable-energy machine, and tests showed it would be difficult to keep the field perturbations small enough in the circulating-beam region. The beam could not jump a magnetic system without using a regenerative field bump-see (v) below.

---

† Work done under the auspices of the U. S. Atomic Energy Commission.

††Permanent address: Swiss Federal Institute of Technology, Zurich.

(iv) An ES channel followed by a magnetic channel. Again this seems complex, and possibly not flexible enough,

(v) Regenerative extraction. The use of an azimuthal field bump either to produce beam spill or enhanced turn separation. Time was not sufficient to make calculations to determine the feasibility of regenerative extraction for our variable-energy machine. Recently Blosser[1]) carried out calculations using our measured field, to see if the efficiency of our existing channel could be enhanced in this way, and we have also made some relevant calculations. At present this question is still open.

As will be seen, calculations on the single-ES channel gave encouraging results.

Computations for some of these possibilities are discussed below. The space devoted to the topics treated is not necessarily related to their relative importance, or to the effort devoted to them, but is also determined by novelty and possible theoretical interest.

2. Multiple Electrostatic Deflectors

At an early stage it became apparent that the simple ES deflector (fig. 1) would be strained to provide sufficient deflection for the highest energy (60-MeV) deuterons. This provided an incentive to consider three deflectors, A, B, C arranged in series, as shown in fig. 2, with their electric fields directed outward, inward, and outward, respectively. The first two deflectors, A and B, produce a large radial amplitude in one turn, so that when the beam enters the third deflector it is headed outward steeply enough to be extracted with a moderate field in deflector C.

Qualitative understanding of such a scheme is obtained from the following simplified linear analysis. We suppose that a sequence of deflectors are all arranged parallel to a reference ray traveling through them, that the electric field is constant in each deflector, and that the magnetic field is uniform.

The departure from the magnetic equilibrium orbit x in a deflector is given by†

$$\frac{d^2x}{d\theta^2} + x = \epsilon \,, \tag{1}$$

where

$$x = \frac{\omega}{c}\,(R - R_0)\,,$$

$$\omega = \frac{eB_0}{m_0 c}\,,$$

$$\epsilon = \frac{E(V/cm)}{300\,B_0\,(G)}\,.$$

The solution of this equation in the deflector at an angle θ from the beginning of the deflector is

$$\begin{pmatrix} x(\theta) \\ x'(\theta) \end{pmatrix} = \epsilon \begin{pmatrix} 1-\cos\theta \\ \sin\theta \end{pmatrix} + M(\theta/0) \begin{pmatrix} x(0) \\ x'(0) \end{pmatrix}, \tag{2}$$

where

$$M(\theta_2/\theta_1) = \begin{bmatrix} \cos(\theta_2-\theta_1) & \sin(\theta_2-\theta_1) \\ -\sin(\theta_2-\theta_1) & \cos(\theta_2-\theta_1) \end{bmatrix}, \tag{3}$$

If the total deflector angle is λ, then the solution at an angle $\theta-\lambda$ beyond the end of the deflector is

$$\begin{pmatrix} x(\theta) \\ x'(\theta) \end{pmatrix} = M(\theta/\theta-\lambda) \begin{pmatrix} x(\lambda) \\ x'(\lambda) \end{pmatrix} = \epsilon\ M(\theta/\theta-\lambda) \begin{pmatrix} 1-\cos\lambda \\ \sin\lambda \end{pmatrix} + M(\theta/0) \begin{pmatrix} x(0) \\ x'(0) \end{pmatrix}$$

$$= \epsilon \begin{pmatrix} \cos(\theta-\lambda) - \cos\theta \\ -\sin(\theta-\lambda) + \sin\theta \end{pmatrix} + M(\theta/0) \begin{pmatrix} x(0) \\ x'(0) \end{pmatrix}. \tag{4}$$

The first term on the right represents the effect of the deflector and is independent of initial conditions, whereas the second represents the motion in the absence of a deflector. Now imagine a sequence of deflectors and gaps with azimuthal length

---

†For an azimuthally uniform cyclotron a more exact equation is $x'' + (1-n+n_e)\,x = \epsilon/\gamma$, where $n = \frac{-RdB}{BdR}$, $n_e = -\frac{2\epsilon}{\beta\gamma}$, $\beta = v/c$, $\gamma = [1-\beta^2]^{-1/2}$.

λ_i, and strength ϵ_i. The ϵ_i may be positive, negative, or zero (for the gaps between deflectors). Then the i^{th} deflector starts at $\theta_{0i} = \sum_{j=1}^{i-1} \lambda_j$ and ends at $\theta_{1i} = \sum_{j=i}^{i} \lambda_j$. From (4) we see that its specific effect at any $\theta \geq \theta_{1i}$ is

$$\begin{pmatrix} x_i(\theta) \\ x'_i(\theta) \end{pmatrix} = \epsilon_i \begin{pmatrix} \cos\left(\theta - \sum_{j=1}^{i} \lambda_j\right) - \cos\left(\theta - \sum_{j=1}^{i-1} \lambda_j\right) \\ -\sin\left(\theta - \sum_{j=1}^{i} \lambda_j\right) + \sin\left(\theta - \sum_{j=1}^{i-1} \lambda_j\right) \end{pmatrix}. \quad (5)$$

One obtains the solution at the end of a sequence of n deflectors (and gaps) by adding the effects of all the deflectors, each of which has an effect given by (5), and then adding the original radial oscillation, $x = A_r \cos(\theta - \phi)$, which goes through unaltered. Thus we obtain (after some rearrangement) the displacement and angle at the end of all the deflectors, at angle $\lambda = \sum_{j=1}^{n} \lambda_j$:

$$\begin{pmatrix} x(\lambda) \\ x'(\lambda) \end{pmatrix} = A_r \begin{pmatrix} \cos(\lambda-\phi) \\ -\sin(\lambda-\phi) \end{pmatrix} - \epsilon_1 \begin{pmatrix} \cos\lambda \\ -\sin\lambda \end{pmatrix} + \epsilon_n \begin{pmatrix} 1 \\ 0 \end{pmatrix} + \sum_{i=1}^{n-1} (\epsilon_i - \epsilon_{i+1}) \begin{pmatrix} \cos\left(\lambda - \sum_{j=1}^{i} \lambda_j\right) \\ -\sin\left(\lambda - \sum_{j=1}^{i} \lambda_j\right) \end{pmatrix}. \quad (6)$$

Let us apply this to the three-deflector system of fig. 2. Suppose deflectors A, B, and the gap between have angular lengths λ_1, λ_3, and λ_2, respectively, and that A, B have equal and opposite electric fields, so that $\epsilon_1 = -\epsilon_3 = \epsilon$, $\epsilon_2 = 0$. The system must satisfy the following conditions:

(i) The end of B must not intercept the circulating beam:

$$x(\lambda_1 + \lambda_2 + \lambda_3) > 0.$$

(ii) When the beam has completed one revolution and enters C it must be outside of deflector A: $x(2\pi) > 0$, and as large as possible.

(iii) The beam should be headed outward, on entering C: $x'(2\pi) > 0$, and as large as possible.

(iv) The deflectors must be outside the dee: $\alpha = \lambda_1 + \lambda_2 + \lambda_3 < \pi$.

What can be concluded from this about the angles λ_1, λ_2, and λ_3? By applying (6) to the above conditions we find, for $A_r = 0$:

$$u = \frac{x(a)}{\epsilon} = -\cos a + \cos(a - \lambda_1) + \cos \lambda_3 - 1 > 0, \quad (7)$$

$$v = \frac{x(2\pi)}{\epsilon} = -\cos a + \cos(a - \lambda_3) + \cos \lambda_1 - 1 > 0, \text{ large}, \quad (8)$$

$$w = \frac{x'(2\pi)}{\epsilon} = -\sin a + \sin(a - \lambda_3) + \sin \lambda_1 > 0, \text{ large}, \quad (9)$$

where

$$a = \lambda_1 + \lambda_2 + \lambda_3 < \pi. \quad (10)$$

One way to see the effect of these conditions is to plot curves of $\cos \lambda_1$ vs $\cos \lambda_3$ for fixed a (see fig. 3). In each case the system point must lie in the triangular region in the upper right. Case (a), $a = 120$ deg, looks most favorable. Case (c), $a = 180$ deg, is impossible.

We used these considerations to suggest several arrangements on which more exact computer runs were based. For these runs we used the MURA III-Tempered Five Code, with Fourier coefficients chosen to fit the model-magnet measured field. The action of the deflectors was simulated by adding or subtracting a constant term from this magnetic field to represent electric field directed inward or outward.

These runs qualitatively confirmed the above analytic estimates of the effect of the first two deflectors. Moreover, on entering the third deflector the beam had not suffered appreciable dispersion. There is considerable dispersion in the third deflector, caused by the fringing field of the magnet, but this affects the single-channel system equally.

Table I shows one three-channel system studied which should give sufficient deflection to 60-MeV deuterons in our cyclotron. The dispersion is indicated in Table 2 by the effect on two rays displaced from the reference ray. The clearance of the reference ray from the undeflected equilibrium orbit is 0.9 in. at the end of channel B, and 1.5 in. at the entrance to channel C.

TABLE 1

Three-channel deflector system

i	Deflector	Interval λ_i (deg)	Angles covered (deg)	Electric field (kV/cm)
1	A	48	0 - 48	100
2	gap	24	48 - 72	0
3	B	48	72 - 120	-100
4	gap	240	120 - 360	0
5	C	144	0 - 144	100

TABLE 2

Dispersion of three-channel system (of Table 1)

	$\Delta R/R$	Δa	$\frac{\Delta R}{R}$	Δa
Start of A	0.005	0	0	0.005
Start of C	0.005	-0.001	-0.0015	0.005
132° down C	0.004	0.004	0.0278	0.042

What has been gained by this system is a limitation of the electric fields to 100 kV/cm, compared to the 160 kV/cm needed for a single channel, with a corresponding increase of channel width by a factor of 2.5 (assuming $V \times E = E^2 d = \text{Const.}$). The price is an enormous increase in mechanical complexity, and use of too much valuable space, so this system was rejected.

3. Analytic Studies of Electrostatic Channel Transmission Efficiency

In this section we present some analytic and graphical methods for estimating the efficiency of electric deflectors. We wished to know how the efficiency depends on particle turn-to-turn separation; on the amplitude and frequency of their radial oscillations; and on channel length, width, and septum thickness.

3.1 CONDITIONS FOR JUMPING THE SEPTUM

We were able to develop a purely analytic treatment for the restricted problem of calculating the fraction of the particles that jump a septum of thickness σ, as a function of radial amplitude A, precessional frequency $\delta = \nu_r - 1$, radial turn-to-turn separation of the equilibrium orbits Δr, and of σ. This efficiency is calculated subject to the assumptions that the internal beam is of uniform density in equilibrium radius, and random in radial oscillation phase, in the vicinity of the deflector.

A septum, of width σ, is located between r_s and $r_s + \sigma$ at $\theta = 0$. We consider a particle of amplitude A at some particular phase Φ of radial oscillation and start counting turns at equilibrium radius $r_0 = r_s - A$. This guarantees that the particle has not previously reached the septum. Actually we cannot specify r_0 this closely since it might vary from $r_s - A$ by an amount Δr (equilibrium radius gain per turn). The first turn is given by

$$r_0(\theta) = r_s - A + \lambda\Delta r + A\cos(\nu_r\,\theta - \Phi),\quad 0 \le \lambda \le 1,\quad 0 \le \Phi \le 2\pi. \qquad (11)$$

After n turns this same orbit will have a radius at the septum azimuth ($\theta = 0$) $r_n \equiv r_n(0)$:

$$r_n = r_s + (n + \lambda)\Delta r - A[1 - \cos(2\pi n\delta - \Phi)],\quad \delta = \nu_r - 1. \qquad (12)$$

All particles in the internal beam are characterized by their values of λ, Φ within the given ranges; our uniformity assumptions imply a uniform density in λ, Φ space. To calculate the efficiency for jumping the septum

we have to calculate the fraction of the λ, $\underline{\Phi}$ rectangle (of area 2π) belonging to particles missing the septum. To do this we rewrite (12) as follows:

$$y_n = \frac{r_n - r_s}{A} = n\,\frac{\Delta r}{A} + z - [1 - \cos(2\pi n\delta - \underline{\Phi}], \quad z = \lambda\,\frac{\Delta r}{A} \tag{13}$$

and ask what fraction of the, $\underline{x}, \underline{\Phi}$ rectangle (of area $2\pi\Delta r/A$) corresponds to particles missing the septum. For each particle there will be a last turn, N, at which it will either jump or hit the septum, defined by the following conditions:

$$y_n < 0, \quad n < N,$$

and

$$\begin{aligned} &y_N > \sigma/A \qquad \text{(jump septum)}, \\ &0 \leq y_N \leq \sigma/A \ \text{(strike septum)}. \end{aligned} \tag{14}$$

It is useful to represent these conditions graphically. This is done in fig. 4 for A = 0.25 in., σ = 0.05 in., Δr = 0.1 in., $2\pi\delta$ = 30 deg. Hence $\sigma/A = 0.2$, $\sigma r/A = 0.4$. To understand the graph the above conditions are written explicitly, using (13), as follows

$$z + n\,\frac{\Delta r}{A} < [1 - \cos(2\pi\delta - \underline{\Phi}], \quad n < N,$$

and

$$[1 - \cos(2\pi N\delta - \underline{\Phi}] \leq z + N\,\frac{\Delta r}{A} \leq \frac{\sigma}{A} + [1 - \cos(2\pi N\delta - \underline{\Phi}], \ \text{hit}$$

$$z + N\,\frac{\Delta r}{A} > \frac{\sigma}{A} + [1 - \cos(2\pi N\delta - \underline{\Phi}], \ \text{jump}. \tag{15}$$

In fig. 4 the abscissa is $\phi_n = \phi - 2\pi n\delta$, the ordinate is $z_n \equiv n\,\frac{\Delta r}{A} + \lambda\,\frac{\Delta r}{A}$. On turn n = 0 all our particles are in the rectangle ADFE. On each successive turn each point $(\underline{\Phi}_n, z_n)$ is displaced by $(-2\pi\delta, \Delta r/A) = \underline{\Delta}$, so rectangle n = 0 moves up to rectangle n = 1, etc. Curves α and β are defined by

$$\alpha: \ (\Phi_n, z_n) = (\Phi_n, 1-\cos\Phi_n),$$
$$\beta: \ (\Phi_n, z_n) = (\Phi_n, \frac{\sigma}{A} + (1 - \cos\Phi_n)), \tag{16}$$

while α_- and α_+ represent the locus of points on α one turn previously and one turn later, respectively (i.e., $\alpha_+ = \alpha + \vec{\Delta}$, $\alpha_- = \alpha - \vec{\Delta}$). Since the conditions (15) are equivalent to

$$z_n < \alpha, \ n < N,$$

$$\alpha \leq z_N \leq \beta, \text{ hit septum,}$$

$$z_N > \beta, \text{ jump septum,}$$

particles between curves α and β hit the septum, and those above β jump the septum provided on the previous turn they were below α. Thus on turn $n = 0$ that part of the rectangle above β represents particles jumping the septum, that part below α represents particles that make another turn, after which they occupy part of the $n = 1$ rectangle -- and again the same three things can happen.

The analysis is simplified by taking the original area to be the dark-shaded zone between α and α_+, rather than the rectangular zone $n = 0$. This is legitimate because both zones have the same area, and every beam particle must pass through each zone. The new zone is $A'B'B''A'' + C'D'D''C''$. The division into two subzones occurs because of the first condition. Point C' is the intersection of curves α and α_-. Had we followed curve α any further to the left beyond C', then on the previous turn the points on α would have been points on α_- above α, contrary to the first condition.

In this way we have chosen a representative zone such that on the previous turn all the particles are in the light-shaded area below α—and thus have not yet reached the septum—while on the turn in question all the representative particles are in the process either of hitting or jumping over the septum.

To calculate the acceptance efficiency $\mathcal{E}$ we take the ratio of the area of the dark-shaded zone above β th that of the total dark-shaded zone, which is the same as that of the original rectangle (with area equal to $2\pi\frac{\Delta r}{A}$):

$$\mathcal{E} = \frac{\text{Area}(a_+ - \beta)}{\text{Area}\,(a_+ - a)} = \frac{\text{Area}(a_+ - \beta)}{2\pi\Delta r/A} \tag{17}$$

This calculation of $\mathcal{E}$ can easily be done by plotting a graph like fig. 4, and using a planimeter to obtain the areas needed. If the precession angle $2\pi\delta \ll 1$, the calculation of $\mathcal{E}$ can also be done analytically as follows. From fig. 5 it is clear that the fraction of particles that hit the septum is

$$\bar{\mathcal{E}} = 1 - \mathcal{E} = \frac{1}{2\pi}\int_0^{2\pi} e\,d\phi, \quad e = \frac{\overline{\Delta B}}{\overline{AC}} = \frac{x_\sigma}{\Delta} \tag{18}$$

To obtain e we write

$$\frac{z_A}{\Phi - \Phi_A} = \frac{1-\cos\bar{\Phi}_A}{\Phi - \Phi_A} = \frac{\Delta r}{2\pi\delta A} = \eta \tag{19a}$$

$$\frac{z_B}{\Phi - \Phi_B} = \frac{1-\cos\bar{\Phi}_B + s}{\Phi - \Phi_B} = \eta, \quad s = \sigma/A, \tag{19b}$$

hence

$$\Delta z = z_B - z_A = \eta(\bar{\Phi}_A - \bar{\Phi}_B) = \eta\Delta\phi\,, \tag{20a}$$

$$\cos\bar{\Phi}_A - \cos\bar{\Phi}_B = \eta(\bar{\Phi}_A - \bar{\Phi}_B) - s = \eta\Delta\bar{\Phi} - s. \tag{20b}$$

If the precession angle $2\pi\delta$ or σ is small enough, $\Delta\bar{\Phi}$ will be small enough to justify replacing $\cos\bar{\Phi}_A - \cos\bar{\Phi}_B$ by $-\Delta\bar{\Phi}\sin\bar{\Phi}_A$, so that from (20) we obtain

$$\Delta\bar{\Phi} \approx \frac{s}{\eta + \sin\bar{\Phi}_A} \tag{21}$$

and

$$x_\sigma = \sqrt{\Delta z^2 + \Delta\phi^2} = \sqrt{\eta^2 + 1} \cdot \frac{s}{\eta + \sin\phi_A} \quad ,$$

$$\Delta = \sqrt{(2\pi\delta)^2 + \left(\frac{\Delta r}{A}\right)^2} = 2\pi\delta\sqrt{\eta^2 + 1} \quad ,$$

whence

$$\varepsilon = x_\sigma/\Delta = \frac{s}{2\pi\delta} \frac{1}{\eta + \sin\phi_A} \quad . \tag{22}$$

From eq. (19a) we have

$$\bar{\Phi} = \bar{\Phi}_A + \frac{1 - \cos\bar{\Phi}_A}{\eta} \quad . \tag{23}$$

This can be used to replace $\bar{\Phi}$ by $\bar{\Phi}_A$ as the integration variable in (18); however, one must exclude those values of $\bar{\Phi}_A$ given by smaller values of $\bar{\Phi}$, otherwise the same $\bar{\Phi}$ values would be counted twice. The excluded region in $\bar{\Phi}_A$, if any, runs from $\bar{\Phi}_{A1}$ to $\bar{\Phi}_{A2}$, where $\bar{\Phi}_{A1}$ is at the maximum of $\bar{\Phi}$ with respect to $\bar{\Phi}_A$, and $\bar{\Phi}_{A2}$ is a larger value of $\bar{\Phi}_A$ for which $\bar{\Phi}(\bar{\Phi}_{A2}) = \bar{\Phi}(\bar{\Phi}_{A1})$. From (23), this means

$$\bar{\Phi}_{A1} = \pi + \sin^{-1}\eta \, , \tag{24}$$

$$\bar{\Phi}_{A2} - \frac{\cos\bar{\Phi}_{A2}}{\eta} = \pi + \sin^{-1}\eta + \frac{\sqrt{1-\eta^2}}{\eta} \, , \quad \bar{\Phi}_{A2} > \bar{\Phi}_{A1} \, .$$

The excluded zone occurs if, and only if, $\eta < 1$. From (23) we have $d\bar{\Phi} = (1 + \frac{1}{\eta}\sin\bar{\Phi}_A)d\bar{\Phi}_A$, so from (18), (22), and (24) we get

$$\Delta = \sqrt{(2\pi\delta)^2 + (\Delta r/A)^2}$$

$$\bar{\mathcal{E}} = \sigma/\Delta r, \qquad \eta > 1$$

$$\bar{\mathcal{E}} = \frac{\sigma}{\Delta r}\left[1 - \frac{\bar{\Phi}_{A2} - \bar{\Phi}_{A1}}{2\pi}\right], \quad \eta < 1 \, . \tag{25}$$

These formulas should be used with some caution because of the approximation (21). The graphical method should be used if more accuracy is desired. It is not surprising that $\bar{\mathcal{E}} = \sigma/\Delta r$ wherever $\eta > 1$, $\frac{s}{\eta - 1} \ll 1$ i.e.

$$\mathcal{E} = 1 - \frac{\sigma}{\Delta r} \qquad (26)$$

wherever

$$2\pi(\nu_r - 1) \ll \frac{\Delta r}{\sigma + A} .$$

3.2 CHANNEL ACCEPTANCE

The graphical method explained above for the septum can now be extended to the whole channel. However, since rather sweeping assumptions are made about the path of the orbits in the channel, we only claim qualitative validity for the results.

Consider the equilibrium orbit that just grazes the septum, with radius $r_e(\theta)$. We start counting turns for a particle with amplitude A, phase Φ, where the crest of its oscillation just touches the septum or is within Δr of doing so. Its displacement from the equilibrium orbit, so long as it is outside the deflector, is x_n^0, where

$$x_n^0(\theta) = r_n(\theta) - r_e(\theta) = (n + \lambda)\,\Delta r - A\,[1 - \cos(2\pi n\delta + \nu_r\,\theta - \Phi)],$$

$$0 \leq \Phi < 2\pi, \quad 0 \leq \lambda \leq 1. \qquad (27)$$

We assume the channel to be shaped for an equilibrium orbit. If the electric field in the channel is constant then the deflected equilibrium orbit (called the reference ray) departs from the undeflected equilibrium orbit roughly quadratically in θ. Hence, the inside edge of the septum, of radius $r_b(\theta)$, is given by $r_b = r_e + x_b$, where $x_b(\theta) = (\frac{\theta}{\lambda})^2 h.$ (28)

Here λ is the azimuthal length of the channel and h is the radial displacement of its end point. We assume that all particles in the channel follow the same path as they would outside, except that we add the deflection term $(\frac{\theta}{\lambda})^2 h$. This assumption is relatively good near the entrance, and gets worse as the channel goes through the cyclotron fringe-field. With this assumption, the displacement of our particle in the channel from the reference equilibrium

orbit is $x_n^{\,i}$, where

$$x_n^{\,i}(\theta) = x_n^{\,0}(\theta) + x_b(\theta). \tag{29}$$

The surfaces of interest are the following, given in terms of their displacement from $r_e(\theta)$ (here d is the channel width and we will sometimes refer to large and small r surfaces as top and bottom, respectively):

$$\begin{aligned}
&\text{end of septum } E_-: && \theta = 0,\ 0 \leq x \leq \sigma \\
&\text{bottom of septum } B_-: && x_b(\theta) = \left(\frac{\theta}{\lambda}\right)^2 h \\
&\text{top of septum } T_-: && x_t(\theta) = x_b(\theta) + \sigma \\
&\text{bottom of electrode } B_+: && x_e(\theta) = x_t(\theta) + d.
\end{aligned} \tag{30}$$

The various things that might happen to a particle on the n^{th} turn are:

(a) strike bottom of septum (B_-) at θ
$x_n^{\,0}(\theta) = x_b(\theta),\quad 0 \leq \theta \leq \lambda$

(a') pass under channel
$x_n^{\,0}(\theta) < x_b(\theta)$

(b) strike end of septum (E_-)
$0 \leq x_n^{\,0}(0) \leq \sigma$

(b') enter channel
$x_n^{\,0}(0) > \sigma$

(c) strike top of septum (T_-) at θ
$x_n^{\,i}(\theta) = x_t(\theta),\quad 0 \leq \theta \leq \lambda$

(c') pass over top of septum
$x_n^{\,i}(\theta) > x_t(\theta),\quad 0 \leq \theta \leq \lambda$

(d) strike bottom of electrode B_+ at θ
$x_n^{\,i}(\theta) = x_e(\theta),\quad 0 \leq \theta \leq \lambda$

(d') pass under electrode
$x_n^{\,i}(\theta) < x_e(\theta),\quad 0 \leq \theta \leq \lambda$

(e) strike end or top of electrode
$x_n^{\,i}(0) \geq x_e(0).$

Transmission on the N^{th} turn requires (a)' for $n < N$, (b)', (c'), and (d') for turn N. Written explicitly, the above conditions, using eqs. (27)-(30), are as follows:

(a)
(a)' $\quad (n + \lambda)\frac{\Delta r}{A} \leq \left(\frac{\theta}{\lambda}\right)^2 \frac{h}{A} + [1 - \cos(\phi - 2\pi n\,\delta - \nu_r\,\theta)]$, any $\theta \leq \lambda$, hit B_-; $0 \leq \lambda \leq \theta$, under B_-

(b) $\quad [1 - \cos(\Phi - 2\pi n\delta)] \leq (n + \lambda)\frac{\Delta r}{A} \leq \frac{\sigma}{A} + [1 - \cos(\Phi - 2\pi n\delta)]$, hit E_-

(b') $\quad (n + \lambda)\frac{\Delta r}{A} > \frac{\sigma}{A} + [1 - \cos(\Phi - 2\pi n\delta)]$, enter channel

$$\left.\begin{matrix}(c)\\(c)'\end{matrix}\right\} : (n+\lambda)\frac{\Delta r}{A} \gtrless \frac{\sigma}{A} + [1-\cos(\phi - 2\pi n\delta - \nu_r\theta)], \quad \begin{matrix}\text{any } \theta \leq \lambda, \\ 0 \leq \lambda \leq \theta,\end{matrix} \quad \begin{matrix}\text{hit } T_- \\ \text{over } T_-\end{matrix}$$

$$\left.\begin{matrix}(d)\\(d)'\end{matrix}\right\} : (n+\lambda)\frac{\Delta r}{A} \lessgtr \frac{\sigma+d}{A} + [1-\cos(\phi-2\pi n\delta - \nu_r\theta)], \quad \begin{matrix}\text{any } \theta \leq \lambda, \\ 0 \leq \lambda \leq \theta,\end{matrix} \quad \begin{matrix}\text{hit } B_+ \\ \text{under } B_+\end{matrix}$$

$$(e) \quad : (n+\lambda)\frac{\Delta r}{A} \geqslant \frac{\sigma+d}{A} + [1-\cos(\phi-2\pi n\delta)], \qquad \text{hit } E_+ \text{ or } T_+.$$

As in the case of septum jumping alone, these conditions may be graphed (fig. 6). Again we want to know what fraction of the (λ, Φ) rectangle corresponds to transmission on some turn n. We plot in $[\Phi - 2\pi n\delta, (n+\lambda)\frac{\Delta r}{A}]$ space the curves bounding the inequalities (a)', (c)', and (d)'. These curves are labeled as follows: α = lower envelope of curves (a), $\beta_1 : (n+\lambda)\frac{\Delta r}{A} = (1-\cos(\Phi - 2\pi n\delta))$, $\beta_2 = \beta_1 + \sigma/A$, γ = upper envelope of curves (c), δ = lower envelope of curves (d), $\epsilon = \beta_2 + (d/A)$.

Again the n = 0 rectangle is the normalizing area, and we replace it by the equivalent zone between curves α and $\alpha+$, where $\alpha+$ is curve α shifted by $\vec{\Delta} = (-2\pi\delta, \Delta r/A)$ as before. This area is broken into subzones as follows:

hit B_-: over α, under β_1

hit E_-: over β_1, under β_2

hit T_-: over β_2, under γ

C (through channel): over γ, under δ

hit B_+: over γ, under ϵ, over δ

T_- or B_+: under γ, over δ (see which curve comes from smallest θ)

E_+ or T_+: over ϵ.

The procedure is to graph all the above curves and mark the areas defined above. The fraction that suffer the various fates described above is obtained by measuring such sub-area, and dividing by the normalizing area $2\pi\Delta r/A$. As before, the total zone $\alpha_+ - \alpha$ might break up into two subzones, broken at the intersection of α and α_-.

Figure 6 illustrates the critical effect precession can have. There are three possible (triangular) zones corresponding to transmission (C). As δ becomes positive, curve a_+ moves into the left hand zone. As δ goes to zero a_+ moves to the right until nothing remains in the left-hand triangle, but some comes in from the upper triangle (this is usually much less). Finally, for large negative $\delta(\nu_r < 1)$, one can exploit the right-hand triangle.

The latter possibility, $\nu_r < 1$, occurs at larger radii as one approaches the maximum of rB(r). Since $p \propto r\,B(r)$, the turn separation Δr is larger there, so curve a_+ is higher than for $\nu_r > 1$, which also enhances transmission. Consequently, δ should either be as positive as possible, or sufficiently negative to get into the right-hand triangle.

A comparison of figs. 6a, b, c, shows the effect of amplitude A on transmission for fixed δ, and the results are combined in fig. 6d. Figure 7 shows a case with negative δ.

3.3 EFFECT OF SPIRAL HILLS

The turn separation Δr at the beginning of the deflector should be maximized in order to enhance jumping of the septum, and this determines the best azimuth for the channel entrance.

If the magnetic field at the septum radius r_0 is written

$$B(r,\theta) = B(r_0)\{1 + \mu' x + \sum_n [a_{3n}\cos(3n\theta) + b_{3n}\sin(3n\theta)] + \dots\},$$

$$x = (r - r_0)/r_0\,, \tag{31}$$

then the equilibrium orbits are given approximately[4] (for a three-sector machine by

$$x_e(\theta) = \frac{1}{8}[a_3\cos(3\theta) + b_3\sin(3\theta)] = \frac{1}{8} f_3 \cos[3(\theta - \theta_H)], \tag{32}$$

where θ_H is approximately at the center of a hill and $f_3 = \sqrt{a_3^2 + b_3^2}$.

The radial gain per turn then is

$$\Delta r(\theta) = \frac{dr_e(\theta)}{dn} = \frac{dr_0}{dn} \left\{1 + \frac{f}{8} \left[\cos 3(\theta-\theta_H) + 3 \tan \Gamma \sin 3(\theta-\theta_H)\right]\right\}, \tag{34}$$

where

$\tan \Gamma = r_0 \frac{d\theta_H}{dr}$ is the spiral angle. For a machine with appreciable spiral, the maximum Δr is near

$$3(\theta-\theta_H) = \pm \pi/2, \text{ for } \Gamma \gtrless 0, \text{ or } \theta \approx \theta_H \pm 30 \text{ deg}. \tag{35}$$

Thus, if the hills are about 60 deg wide, we see that the channel should start at the end or beginning of a hill, depending on whether the spiral is with or against the particle rotation, respectively.

Of course the choice of initial angle will also affect the amount of radial deflection attainable with a given electric field. For low energy machines the beam might be deflected sharply enough to have most of the deflector in a valley. Then, perhaps one should have the spiraling with the particle rotation and start deflection at the beginning of a valley, so that both turn separation and deflection will be optimized. For higher energies the deflector runs through both hill and valley, and the deflection is less sensitive to position of the deflector, especially if the spiral is against the particle rotation.

It is not completely obvious that spiral in the particle-rotation direction is best, for while it means deflection can start in a valley, the orbit is headed inward there. Also, the hill field falls off faster with radius. For our cyclotron the spiral is counter to the particle rotation, a choice not entirely governed by deflector considerations.

4. Channel Efficiency Computer Studies

4.1 DEFLECTION CODE CYBOUT

To facilitate more precise predictions of channel efficiency a specialized computer code for the IBM 704 was designed by one of the authors, and written by Owens[2]) at Oak Ridge National Laboratory. This code, called CYBOUT, is intended both to calculate channel wall coordinates and transmission efficiencies.

The heart of the CYBOUT code is the Oak Ridge general orbit code GOC, which integrates orbits in a magnetic field specified on a polar-coordinate grid in the median plane. The effect of an electric channel is represented by an appropriate change in the original magnetic field, which is valid if the channel follows the orbits, so that the electric field is always perpendicular to them. The effect of a magnetic channel is also specified by an appropriate field modification. First-harmonic perturbation of the field for regenerative extraction can be introduced by specifying the amplitude and phase of the first harmonic as functions of radius.

For an electric channel one gives the electric field in the form

$$E(\theta) = E_0 + E_1(\theta-\theta_0) + E_2(\theta-\theta_0)^2, \qquad (36)$$

where θ_0 is the entrance azimuth of the channel. A reference ray is chosen by specifying initial conditions p, r_i, p_{ri} at some $\theta_i \leq \theta_0$. The code integrates this reference orbit into and through the channel (from θ_0 to θ_1), and beyond to θ_f. From this information and the specification of deflector voltage V_e and septum thickness σ, a trial configuration of the channel is calculated and stored by the computer.

To estimate acceptance efficiency, one specifies initial conditions for a representative set of orbits at radii sufficiently smaller than that of the channel to be sure they have not yet hit it. Each orbit is then integrated with acceleration; and the computer keeps track of whether each orbit stays

outside the channel, strikes some part of the septum, or enters the channel. If the particle enters the channel, its orbit is integrated through the E-modified magnetic field. The integration stops when the orbit hits the septum or electrode, or goes through the channel (to θ_f). By recording, with CYBOUT, the fates of a sufficiently large and representative set of particles, one may estimate the efficiency of the channel.

The addition to, or replacement of, the electric field in the channel by a field change caused by a magnetic channel simply alters the effective field within and outside the channel. Addition of a first-harmonic bump modifies the field everywhere. The code can also simulate the effect of several channels in series.

4.2 NUMERICAL CALCULATIONS

Most of our numerical calculations with the CYBOUT code were concerned with the design of a single ES channel for 60-MeV deuterons, since these particles require the largest electric field. It will be recalled that the graphical analysis yielded good channel acceptance either for small positive precession, or for large negative precession. The latter corresponds to ES extraction from conventional cyclotrons, and a major objective of our analysis was to determine the feasibility of extraction with positive precession. We considered this a safer way to extract, since we feared it might prove impossible to bring the beam through the $\nu_r = 1$ and $\nu_r = 2\nu_z$ resonances which would occur before δ was sufficiently negative to provide good channel efficiency. Consequently, we began our studies with the code putting the channel at 37 in. where $\nu_r \approx 1.03$.

The first task was to determine values of E_0, E_1, E_2 [eq. (36)] that would give an external beam 5 to 10 in. away from and parallel to the yoke. This was done by trial-and-error variation of the E_i, and plotting of the external orbits. Then one sets the electrode voltage V_e at a value given

by the empirical sparking limit:

$$V_e E = K = \text{constant}. \qquad (37)$$

This constant is about $10^4 kV^2/cm$ for copper, and perhaps twice that for hot glass. Since the channel is usually narrowest at the start, this limit controls E_0 only. (It is important to deflect as much as possible at the beginning, since this is most effective in terms of maximizing displacement at the channel exit.)

After we had obtained suitable values of the E_i, acceptance studies were made. These involved 'shooting' representative particles at the deflector, as described above. We computed orbits for five different energies, spanning ΔE, the energy gain per turn; we took at each of those energies initial values of r, p_r located on a rectangular grid about the equilibrium orbit for the energy involved. These grids generally included radial amplitudes of 1/16, 1/8, and 1/4 in.

For these studies at 37 in. the relevant parameters were typically $\nu_r = 1.03$, $\Delta r = 0.04$ in. (for 70-kV dee voltage), $\sigma = 0.03$ in., $\lambda = 108$ deg, $E_0 \approx 185$ kV/cm, $V_0 = (10^4/185)$ kV. We found the results were quite sensitive to various parameters at our disposal. Thus toward the end of the channel the beam is dispersed most strongly by the fringe-field. Consequently one gains a good deal by flaring the channel at the downstream end to conform to the beam envelope. It was best to tilt the channel inwards relative to a deflected equilibrium orbit which has entered the deflector. It was also advantageous to run the reference ray much closer to the inside of the channel than to the outside. We found that with the parameters noted above we were able to obtain extraction efficiencies of 10 to 15% for amplitudes up to 1/8 in.

This acceptance is perhaps satisfactory, but not outstanding. Meanwhile we had been urged by Richardson[3]) to try larger radii, since his experience with the Berkeley electron model had convinced him that

particles would spill without any assistance. If the beam could negotiate the resonances, channel efficiency should improve at larger radii because the turn separation increases near the peak of rB(r), the precession becomes strongly negative, and less E-field is required to deflect, allowing the channel to be wider. Therefore we decided to try CYBOUT acceptance runs further out, and investigate the resonances later.

The CYBOUT code was used with the channel entrance at 38, 38.5, and 39 in. For 38 in. we obtained essentially zero acceptance -- as expected from the graphical analysis, because δ was negative but small. However at 38-1/2 and 39 in., especially 39 in., we obtained very encouraging results. At 39 in. the turn separation Δr had increased to about 0.06 in., $\nu_r \approx 0.8$, and E ≈ 65 MeV. We took a reference ray 1/16 in. outside and headed inward by (1/16 in./r)radians relative to the corresponding equilibrium orbit, and used a flared channel shape: $E = (160-35\theta^2)$kV/cm, (this shape fits the 1/8 in. amplitude orbits fairly well). With this configuration we were able to obtain about 50% transmission efficiency for particles with A ≤ 1/8 in., and about 20% for A ≈ 1/4 in. This regime of extraction corresponds to the graphical analysis of fig. 7. The energy spread of the transmitted particles is 0.3 to 0.4 MeV. These particles leave the channel as if they originated at a point source about 3/4 in. upstream from the channel exit, with an angular spread of 1/2 deg. The point source moves inward with energy at a rate of about 0.1 in./MeV. The moderate effect of the fringe-fields in the channel on the axial motion is shown on three sample orbits in fig. 8.

There are possible hazards to extraction at 39 in. One is that the beam will be lost vertically near 38 in., where the coupling resonance $\nu_r = 2\nu_z$ occurs. Another is that the radial beam quality will deteriorate in passing through the $\nu_r = 1$ radial resonance. For reasons that will be discussed in the next section, neither of these effects should be too bad; the channel was

designed for extraction at 39 in. but considerable flexibility has been provided. It is 108 deg long, and is jointed at 72 deg. Each of the six relevant points, two at each end and two at the joint, can be moved about 3 in. in radius.

The proper shaping of the channel field and choice of reference ray was accomplished, needless to say, after considerable experimentation with CYBOUT, plotting of deflected orbits, etc.

Unfortunately, the optimal channel shape for high-energy deuterons is not optimal for particles in lower fields. This problem has not yet been fully explored by calculations; however, it is less severe because at lower fields the deflecting field can be weaker, and the channel wider. A preliminary calculation showed that 50 MeV protons, at about 12 kG, would fit in the channel. It is possible that an additional element of flexibility in the system may be required to prevent interference of the septum with the circulating beam under these conditions.

The statistics of our acceptance run with the 39-in. channel are shown in figs. 9 and 10, the first showing the energy spread in fractions of 140 keV (one turn), and the second the fractions of particles that go through the channel, hit the septum, etc., vs amplitude.

5. Transition Through the Resonance Region

5.1 RADIAL STABILITY

It is not certain that the beam can be accelerated out to a radius where ν_r is sufficiently less than one to exploit the right-hand acceptance triangle (fig. 6a) while retaining adequate radial and axial beam quality. In our cyclotron at least, there is no problem with phase lag, which is about 30 deg at 39 in., where $\nu_r \approx 0.8$. As for loss of radial beam quality, acceleration runs on the GOC (general orbit code) showed that the beam suffers hardly any distortion on passing through $\nu_r = 1$ for $A \leq 1/8$ in., and only moderate distortion up to 1/4 in. (see fig. 11).

However, if there is a small first-harmonic component in the field, a large radial oscillation will be introduced. This effect may be estimated as follows. The radial equation of motion may be written approximately

$$\frac{d^2x}{d\theta^2} + \nu_r^2 x = \frac{B_1}{B_0} \cos\theta, \tag{38}$$

where B_0 and B_1 are the azmuthal average and first-harmonic amplitude of the field, respectively, and

$$x = (r - r_0)/r_0 .$$

We approximate ν_r near the resonance by

$$\nu_r = 1 - \epsilon\,\theta. \tag{39}$$

Integration of the resulting equation involves a Fresnel integral. Most of the change in x occurs over a comparatively small range in θ, so one gets the correct shift approximately by integrating between $\pm\infty$. The result is that traversal of the $\nu_r = 1$ radius with a first-harmonic component B_1 induces a radial amplitude

$$A_r = R\,\frac{B_1}{B_0}\,\sqrt{\frac{\pi}{\epsilon}}\,. \tag{40}$$

The quantity $\epsilon = d\,\nu_r/d\theta$ can be obtained, for example, by running the equilibrium orbit code at equal small increments of energy. For 60-MeV

deuterons in our cyclotron, with 70-kV dee voltage, we have R = 37 in., $B_0 = 17 \times 10^3$ G, whence $A_r \approx (1/7)B_1$ in. This estimate was well-confirmed by the orbit code.

There are two bad consequences of having such a radial amplitude. The first is that if the ES channel has been shaped as described in sec. 4.2, it will not accept large amplitudes. Thus our calculations showed acceptance dropping from 50% to 20% between 1/8 in. and 1/4 in. amplitude, and reaching zero at about 3/8 in. Second, the energy of radial oscillation can feed into that of vertical oscillation when $\nu_z = \nu_r/2$. This occurs at about 38 in. in our cyclotron, before the optimal radius for channel acceptance.

5.2 AXIAL STABILITY

The coupling (Walkinshaw) resonance at $\nu_x = 2\nu_y$ is a formidable barrier, and it is usually regarded as impassable.* However, this resonance can be passed if the fringe-field is suitably shaped, since both the strength of the driving force at the resonance and the resonance width depend critically on the radial derivatives of the average magnetic field and on the amplitude of radial oscillation.

In our cyclotron, the Walkinshaw resonance is never traversed in the isochronous region of the magnetic field, but only in the fringe-field, where the large negative gradient of the average field causes ν_y to become large. In this region the strongest nonlinear terms in both radial and axial motion arise from the average field only.

We shall analyze the effect neglecting flutter and comment briefly on its influence at the end. We keep only the largest nonlinear terms in the fringe-field region and find that the equations for $x = (r - r_0)/r_0$, $y = z/r_0$ are approximately

$$\frac{d^2x}{d\theta^2} + \nu_x^2 x = \frac{\mu''}{2}(y^2 - x^2) + \frac{\mu'''}{2} xy^2 - \frac{\mu'''}{6} x^3 , \tag{41a}$$

$$\frac{d^2y}{d\theta^2} + \nu_y^2 y = \mu'' xy + \frac{\mu'''}{2} x^2 y - \frac{\mu'''}{6} y^3 . \tag{41b}$$

where $\mu^{(n)} = (r_0^n / B(r_0))(d^n B(r_0)/dr_0^n)$. In these equations and in the subsequent analysis we assume that $\mu''' \gg \mu'' \gg \mu'$. Equations (41) follow from a Hamiltonian

$$H = \left(\frac{p_x^2}{2} + \frac{p_y^2}{2}\right) + \left[\frac{\nu_x^2}{2} x^2 + \frac{\nu_y^2}{2} y^2 - \frac{\mu''}{2} x\left(y^2 - \frac{x^2}{3}\right) + \frac{\mu'''}{24}(x^4 - 6x^2y^2 + y^4)\right] . \tag{42}$$

---

*We have changed notation here, and now write ν_x and ν_y in place of ν_r and ν_z.

The topology of the equipotential curves of the potential energy function in the x-y plane is determined by the location and character of the stationary points of $V(x, y)$. We have examined these under the assumptions (1) $\nu_x \simeq 2\nu_y$, (2) $\mu''' < 0$, and (3) $(\mu'')^2/(\mu''' \nu_y^2) \equiv a \ll 1$.

V has a minimum value at the origin, which is surrounded by a set of closed equipotential lines. The saddle points nearest the origin are at

$$x = -\frac{3}{7}\frac{\mu''}{\mu'''}\left[1 + O(a)\right], \quad y = \pm\left\{-\frac{6\nu_y^2}{\mu'''}\left[1 + 0.34\,a + O(a^2)\right]\right\}^{1/2}.$$

They are connected by an equipotential line, inside of which all equipotentials are closed and outside of which they diverge to infinity. The maxima in x and y of the enclosed region are given approximately by

$$x_{max}^2 \simeq -\frac{3\nu_y^2}{4\mu'''}\left[1 + 0.41a + O(a^2)\right],$$
$$y_{max}^2 \simeq -\frac{6\nu_y^2}{\mu'''}\left[1 + 0.34a + O(a^2)\right]. \tag{43}$$

The coefficients in these formulas are evaluated for $\nu_x = 2\nu_y$ and approximated numerically. (The next terms in the series contribute less than 20% for $|a|$ as large as 1.4.)

At $\nu_x = 2\nu_y$ we find from (43) that for small μ'', $y_{max}/x_{max} \simeq 8^{1/2}$, the ratio of extreme displacements is smaller for equipotentials lying nearer the origin. Since the available aperture allows only $z < 3/4$ in., we must keep $A_r < 1/4$ in. to avoid beam loss if the particles stay within the stopband long enough to transfer an appreciable fraction of the energy from x to y motion. Consequently, safe passage of the coupling resonance is assured for our cyclotron conditions provided the orbits are centered within 1/4 in. and have incoherent radial oscillations with amplitudes under 1/4 in. at the extraction radius.

The situation would have been worse had y_{max}, eq. (43), been smaller; it can be seen from eq. (41) that the axial force is defocusing for $y \tilde{>} y_{max}$ even if $x = 0$. However, since our aperture is much less than y_{max}, we may proceed by regarding the nonlinear terms in eq. (41) as perturbations and assuming the amplitudes and phases of the x and y oscillations to be slowly varying parameters, as follows:

$$x = A_x \sin(\nu_x \theta + \psi_x), \quad p_x = \nu_x A_x \cos(\nu_x \theta + \psi_x), \tag{44}$$

and similarly for y. We obtain the equations of motion for A_x, A_y, ψ_x, and ψ_y, retaining only terms of low frequency, $\sigma = 2\nu_y - \nu_x$.

$$\frac{dA_x}{d\theta} = -\frac{\mu''}{8\nu_x} A_y^2 \cos\chi,$$

$$\frac{dA_y}{d\theta} = \frac{\mu''}{4\nu_y} A_x A_y \cos\chi, \tag{45}$$

$$\frac{d\psi_x}{d\theta} = -\frac{\mu''}{8\nu_x} \frac{A_y^2}{A_x} \sin\chi + \frac{\mu'''}{8\nu_x} \left(\frac{A_x^2}{2} - A_y^2\right),$$

$$\frac{d\psi_y}{d\theta} = -\frac{\mu''}{4\nu_y} A_x \sin\chi - \frac{\mu'''}{8\nu_y} \left(A_x^2 - \frac{A_y^2}{2}\right),$$

where $\chi \equiv \sigma\theta + 2\psi_y - \psi_x$. This system may be shown to have two invariants, A and C, defined by

$$4A^2 = 4A_x^2 + A_y^2 \tag{46a}$$

and

$$C = \frac{\mu''}{\nu_x} A_y^2 \sqrt{A^2 - A_y^2/4} \sin\chi - (\sigma - \sigma_0)A_y^2 - \frac{33\mu'''}{128\nu_x} A_y^4, \tag{46b}$$

where

$$\sigma_0 = \frac{9\mu''' A^2}{16\nu_x} ,$$

and we have set $\nu_x = 2\nu_y$ in the various coefficients. The assumptions underlying this treatment are valid only if $A^2 < -3\nu_x^2/(8\mu''')$.

From eq. (46b) one may see that A_y^2 will oscillate between limits A_{y1}^2 and A_{y2}^2, positive solutions of the quartic equation for A_y^2 obtained by setting $\sin\chi = \pm 1$ in eq. (46b). The limits A_{y1}^2 and A_{y2}^2 are close together for $|\sigma - \sigma_0| > |\frac{\mu'' A}{\nu_x}|$, corresponding to little change of axial amplitude, but if $|\sigma - \sigma_0| < |\frac{\mu'' A}{\sigma_x}|$ they may be quite far apart, and most of the oscillation energy may go into the axial mode. Thus the equations $\sigma - \sigma_0 = \pm |\frac{\mu'' A}{\nu_x}|$ define the edges of the stopband, whose center is located at the radius where $\sigma = \sigma_0$. Since $d\sigma/dr > 0$ and $\mu''' < 0$ we see that the resonance occurs at smaller radii for larger values of A.

As particles are accelerated the parameters σ, μ'', μ''', and ν_x change continuously. Since σ changes most rapidly, the stopband width corresponds to an azimuthal interval θ_s given approximately by

$$\theta_s \approx \left| \frac{2\mu'' A}{\nu_x \, d\sigma/d\theta} \right| . \qquad (47)$$

To calculate the maximum value of A_y one could integrate equations (45) allowing for the slow variations of all the parameters. Instead, we will estimate this value by neglecting energy interchange outside the stopband but including it at the maximum rate (that at the stopband center) everywhere inside the stopband. The azimuthal interval θ_s required for one interchange from the smallest value of A_y to the largest (from A_{y1} to A_{y2}) may be obtained as an elliptic integral involving all of the parameters appearing in eqs. (46). We are most interested in the case that initially most of the energy is radial; i.e. $A_{y1}^2/4A^2 \ll 1$. In this case $A_{y2}^2/4A^2 \approx 1$; i.e. most of the

energy becomes axial. For this case the elliptic integral for θ_e (at the stopband center $\sigma = \sigma_0$) may be written approximately

$$\theta_e \approx \frac{\nu_x}{\mu'' A} \ln\left(\frac{32A^2}{A_{y1}^2}\right). \tag{48}$$

A similar result has been obtained by J. W. Burren.[7])

If $\theta_s > \theta_e$ the stopband is wide enough to allow a complete interchange. This condition is found from eqs. (47) and (48) to be

$$\frac{2(\mu'' A)^2}{\nu_x^2 \, d\sigma/d\theta} > \ln\left(\frac{32A^2}{A_{y1}^2}\right) \tag{49}$$

with the parameters evaluated at the stopband center; it may also be expressed in terms of the energy gain per turn, $m_0c^2 \epsilon_0 \cos\phi_{rf}$, as

$$\frac{8\pi\beta^2\gamma^3 |\mu''| A^2}{5\nu_x \epsilon_0 \cos\phi_{rf}} > \ln\left(\frac{32A^2}{A_{y1}^2}\right), \tag{50}$$

where it has been assumed that $\nu_y^2 \approx -\mu'$ and $\nu_x^2 \approx 1 + \mu'$. Therefore $|\mu''|$ should be kept small in the stopband to avoid large axial growth for relevant values of $A(\sim A_x)$. Typical values for 60 MeV deuterons in our cyclotron are $\mu'' \sim -6$, $\beta \doteq 0.18$, $\epsilon_0 \sim 3.5 \times 10^{-5}$, yielding $A_x > 0.4$ in. for complete interchange when $A_{y1} \sim 1/4$ in.

With suitably shaped fields beam spill may occur before the resonance is reached if A_x is large. It is also possible that for large A_x the resonance may be shifted inward so far as to occur at a radius where $|\mu''|$ is small enough to avoid complete interchange. For these reasons particles with large radial amplitudes need not always be lost.

The influence of flutter is to modify the coefficients μ'' and μ''' in eqs. (45)-(50). A large number of terms play a role, including terms involving third derivatives of the flutter, and cross terms with flutter and μ'''. The possibility exists of reducing the effective value of $|\mu''|$ by a suitable choice of field parameters in the extraction region.

One other resonance should be mentioned. If a first harmonic field component is present, an axial instability exists at $\nu_y = 1/2$ because of the μ'' coupling of the axial motion to the distorted equilibrium orbit. The amplitude of the driving term is approximately $A_x = (B_1/B_0)(1 - \nu_x^2)^{-1}$. For our cyclotron $1 - \nu_r^2 = 0.1$ where $\nu_y = 1/2$, which is at a slightly larger radius than the $\nu_x = 2\nu_y$ resonance. At $\nu_y = 1/2$, a 10 gauss first harmonic gives $A_r = 1/4$ inch. Since such a first harmonic would induce about one inch of radial amplitude (of frequency ν_x) in passing through $\nu_x = 1$, the $\nu_y = 1/2$ resonance is far less important than the $\nu_x = 2\nu_y$ resonance.

5.3 USE OF FIRST HARMONIC TO AID EXTRACTION

Some orbit computations have been carried out corresponding to the situation in which beam spill was induced by Richardson.[6]) He energized the outer valley correcting coils so that they produced a first-harmonic amplitude rising slowly from 30 in. to a peak of about 20 G at 37 in., with the peak of the bump 140 deg upstream from the deflector entrance. The computed orbits developed radial amplitudes of about 3 in. at about 37 in., and then spilled (one third of them into the dee, however). The divergence of the spill-beam was very large. However, a few turns before the spill, and near the deflector-entrance azimuth, the orbits were very concentrated in r, p_r space. They also showed complete turn-to-turn separation (for an initial 1/8-in.-amplitude distribution) and jumped sufficiently to enter the channel with almost 100% efficiency. Unfortunately, these orbits also have about 10% less energy than they would without a field bump. This in itself means that a higher electric field might be required to deflect them, but on the other hand the larger radial momentum of the bumped orbits reduces the field required. Further investigation of this possibility is planned.

Acknowledgments

Many other persons have contributed to the theoretical work on our deflection system. We wish to thank H. G. Blosser who has calculated many radial phase plots and explored regenerative extraction possibilities for our cyclotron. We have profited from collaboration with members of the ORNL staff, R. H. Bassel and R. S. Bender and wish especially to acknowledge their cooperation in design and coding of the CYBOUT deflection code. We also wish to thank F. T. Cole and E. Chapman of MURA for providing us with the Ill Tempered Five orbit code. E. L. Kelly and J. R. Richardson have contributed extremely valuable help through their interest, knowledge and advice. It is with the greatest pleasure that we thank the following members of the Computing group who wrote many of the codes used and carried out the numerical computations involved in these deflection studies: A. S. Kenney, H. C. Owens, J. D. Young, and D. R. Brainard.

REFERENCES

[1]) H. G. Blosser (Michigan State University) private communication.

[2]) H. G. Owens, Three Computer Programs for Calculating Cyclotron Orbits, Lawrence Radiation Laboratory Report UCRL-10083, April 1962, Nucl. Instr. and Meth. (to be published).

[3]) J. R. Richardson (University of California at Los Angeles) private communication.

[4]) Lloyd Smith and A. A. Garren, Orbit Dynamics in the Spiral-Ridged Cyclotron, Lawrence Radiation Laboratory Report UCRL-8898, Jan. 1959 (unpublished).

[5]) H. C. Owens and T. A. Welton, An IBM 704 Code for Studying Particle Orbits in Cyclotron Fields, Oak Ridge National Laboratories Report CF 59-11-3, Nov. 1959 (unpublished).

[6]) J. R. Richardson, paper presented at the International Conference on Sector-Focused Cyclotrons, Los Angeles, April 1962, Nucl. Instr. and Meth. (to be published).

[7]) J. W. Burren, Vertical Motion in Spiral Sector Accelerators, Harwell laboratory report AERE T/R 2423.

FIGURE CAPTIONS

Fig. 1. Schematic diagram of single electrostatic deflector for the Berkeley 88-inch cyclotron.

Fig. 2. Schematic diagram of triple ES deflector system.

Fig. 3. Graphical construction for three-deflector system [see eqs (7)-(10)]. λ_1 = length of channel A(deg), λ_2 = gap A-B, λ_3 = length of B, $\alpha = \lambda_1 + \lambda_2 + \lambda_3$. Each plot shows λ_3 vs λ_1, for fixed α. Conditions (7)-(10) require that point (λ_1, λ_3) be away from hatched side of each curve, and restrict point to be in triangular region at upper right. (Fig. 3a: $\alpha = 120^\circ$, fig. 3b: $\alpha = 150^\circ$, fig. 3c: $\alpha = 180^\circ$.)

Fig. 4. Graph representing efficiency for jumping a septum of width σ, by particles with turn separation Δr, amplitude A, precession frequency $\delta = \nu_r - 1$. This graph represents $2\pi\delta = 30^\circ$, $\sigma/A = 0.2$, $\Delta r/A = 0.4$, (see Text).

Fig. 5. Diagram to indicate derivation of approximate formula for septum-jumping efficiency.

Fig. 6a. Graphical construction for ES channel efficiency. Shaded areas are proportional to the fraction of particles striking various parts of the deflector or passing through, according to letter key in schematic diagram at upper right. Normalizing area (all shaded area) = $360 \cdot \Delta r/A$ degrees. Unshaded lettered areas are potentially available, by changing $\Delta r/A$ or δ.

Fig. 6b. Channel acceptance for 1/16-in. radial amplitude. Other parameters are the same as for fig. 6a.

Fig. 6c. Channel acceptance for 1/4-in. radial amplitude. Other parameters are the same as for fig. 6a.

Fig. 6d. Channel transmission efficiency vs amplitude from graphs 6a, b, c.

Fig. 7. A channel acceptance diagram for $\nu_r < 1$.

Fig. 8. Axial motion in deflector channel.

Fig. 9. Energy and amplitude distribution of particles transmitted by channel at 39 in. from computer runs. Integration of all orbits was begun about 1/2 in. inside of channel, with energy spread corresponding to one turn (140 kV). Turn number is number of turns orbits made before entering channel. Shadings represent different radial amplitudes.

Fig. 10. Percentage of particles transmitted by channel or striking various parts of structure, as functions of radial amplitude.

Fig. 11a. Radial distortion of particles accelerated through $\nu_r = 1$ (at 37.5 in.); amplitude of grid = $\frac{1}{8}$ in.

Fig. 11b. Radial distortion of particles accelerated through $\nu_r = 1$ (at 37.5 in.); amplitude of grid = $\frac{1}{4}$ in.

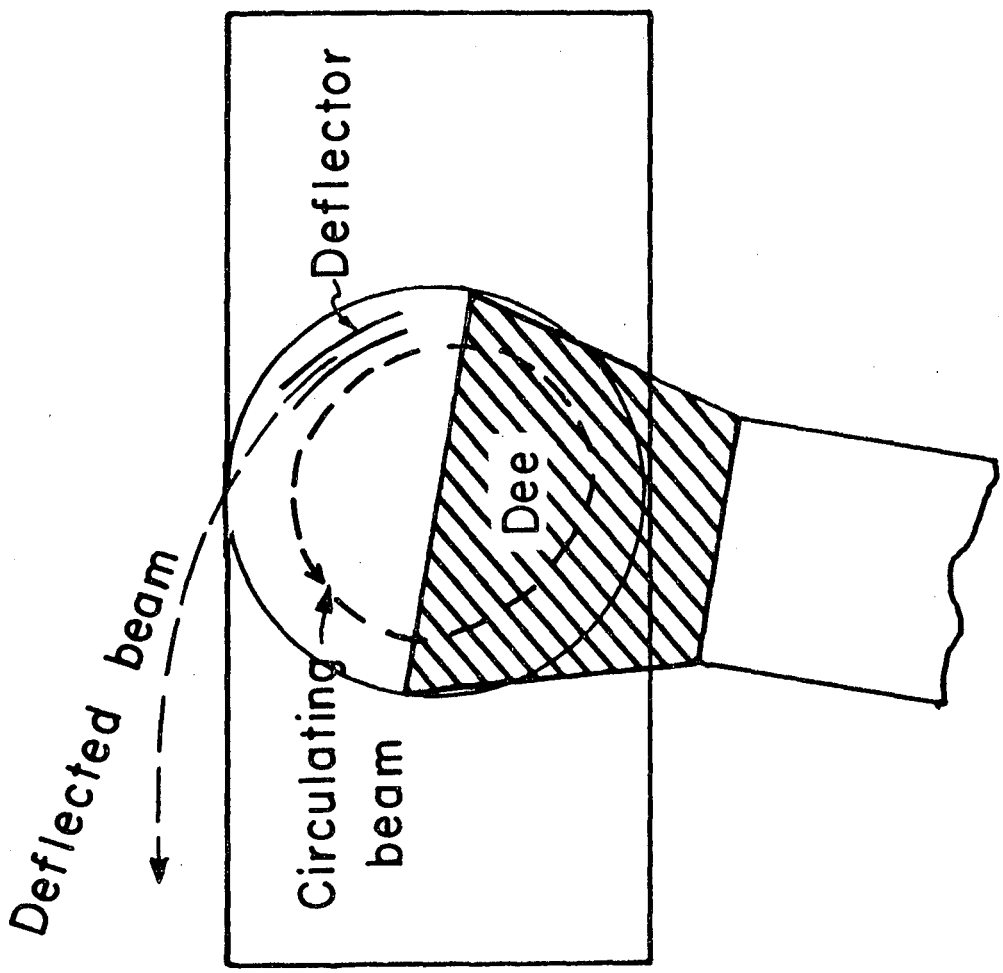

MU-26364

Fig. 1

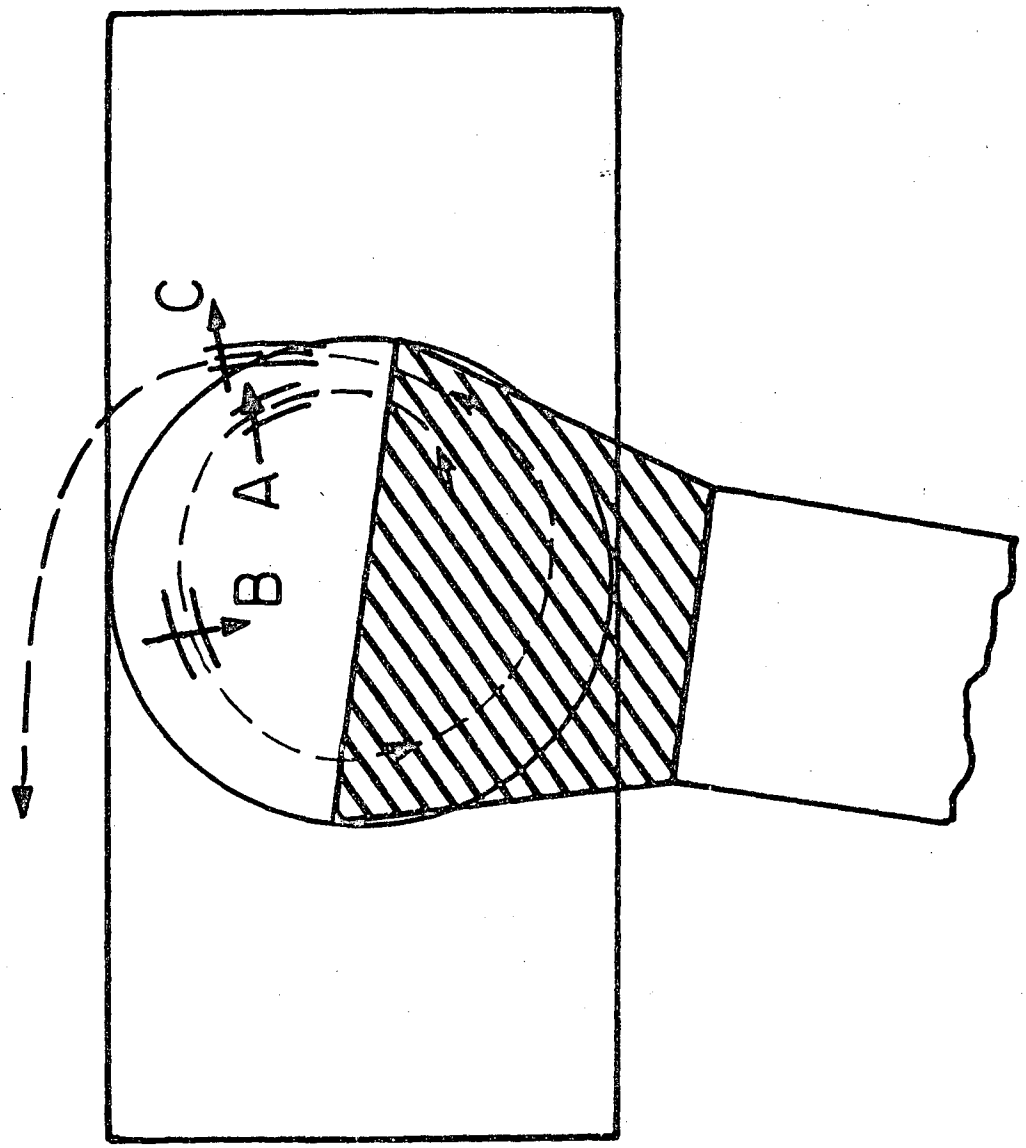

MU-26363
Fig. 2

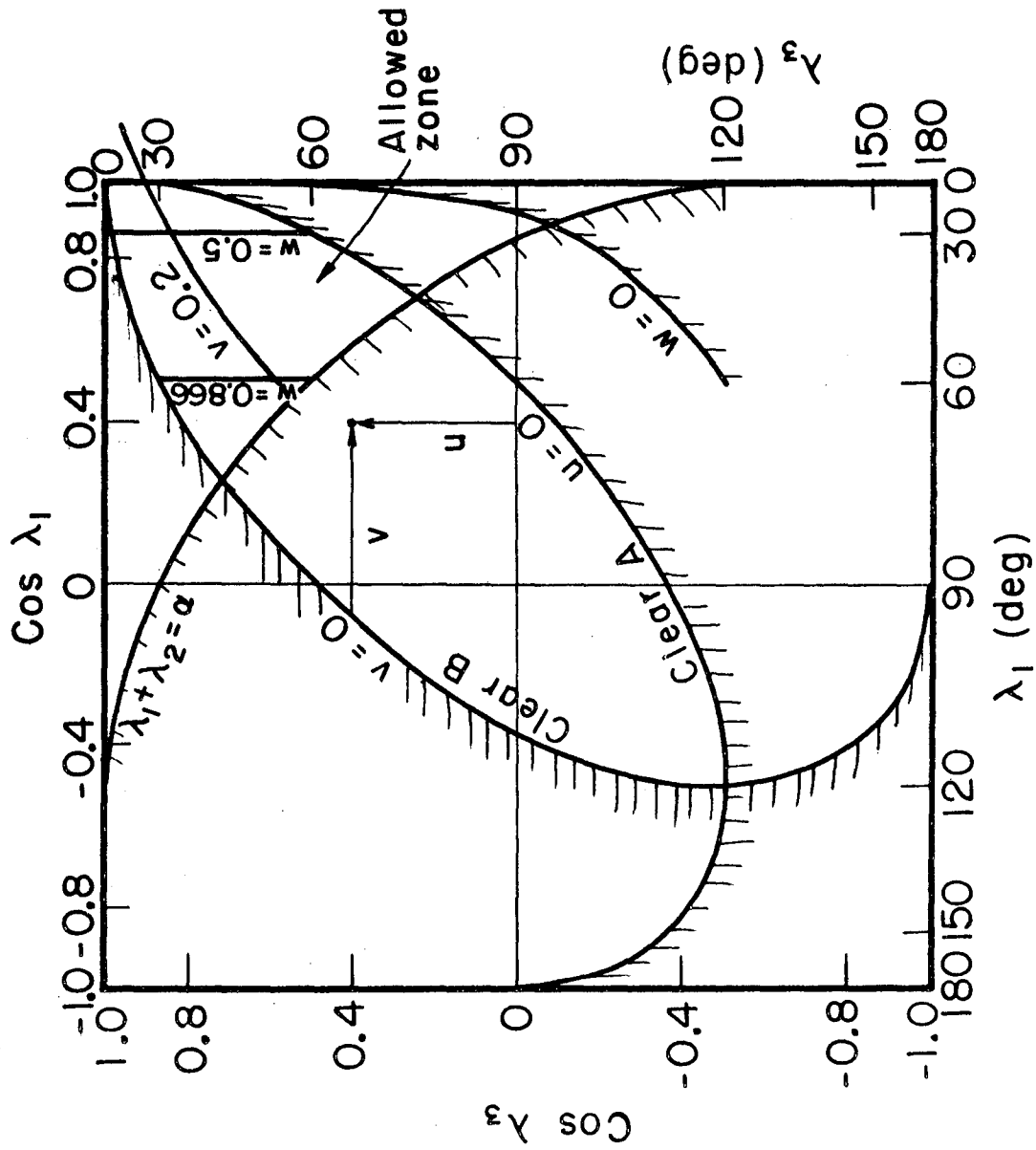

MU-26395

Fig. 3a

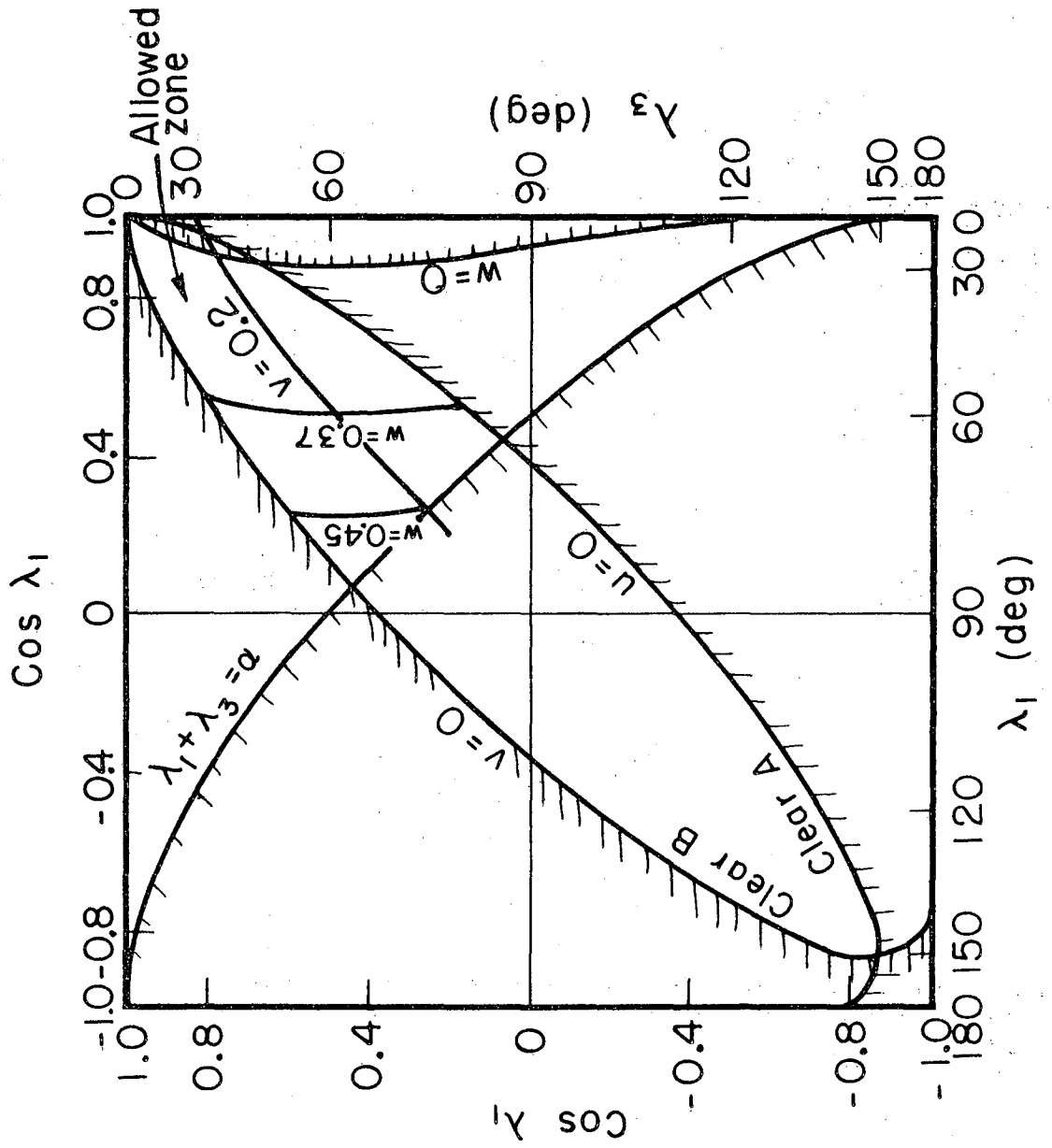

MU-26396
Fig. 3b

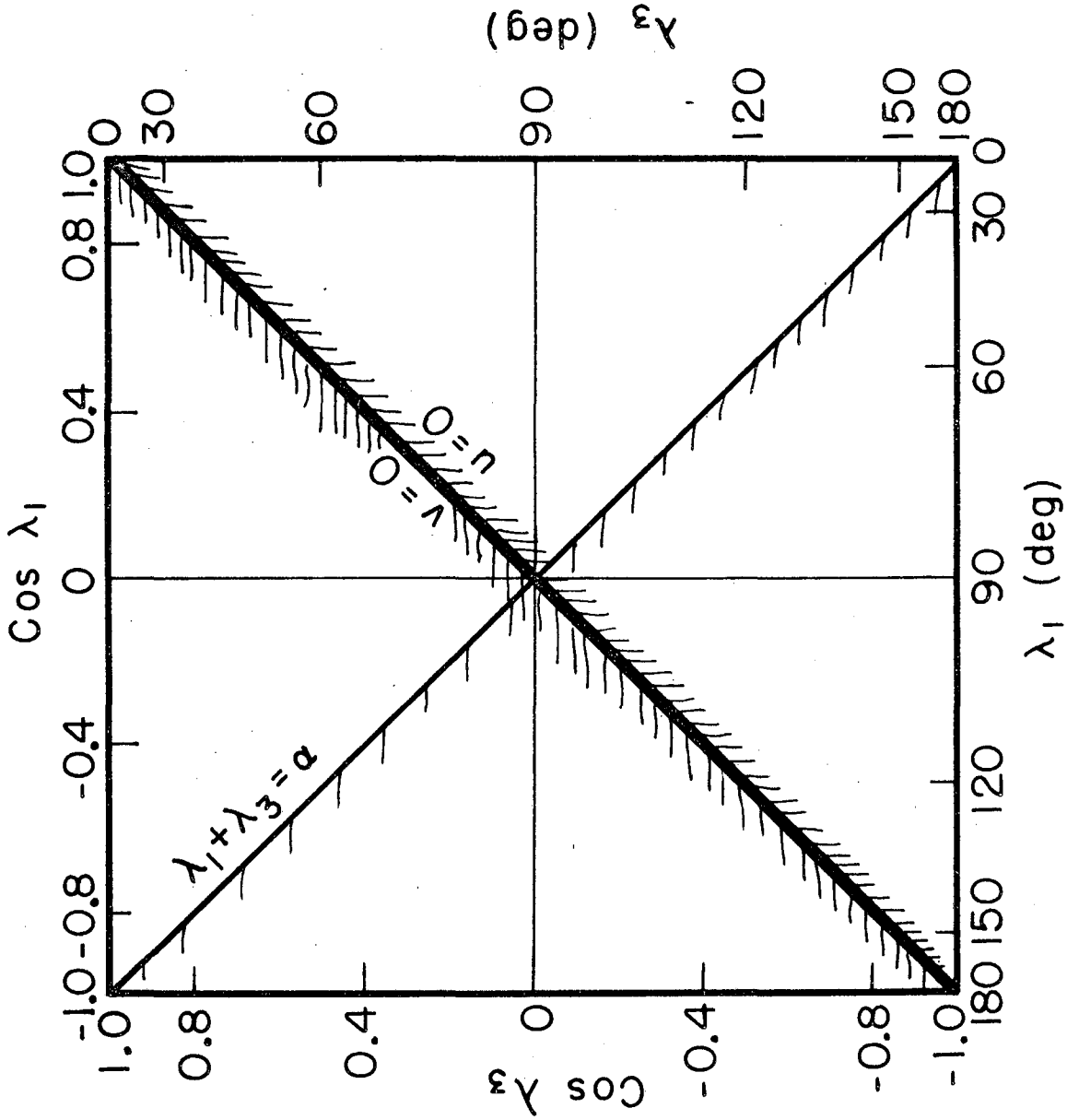

MU-26390
Fig. 3c

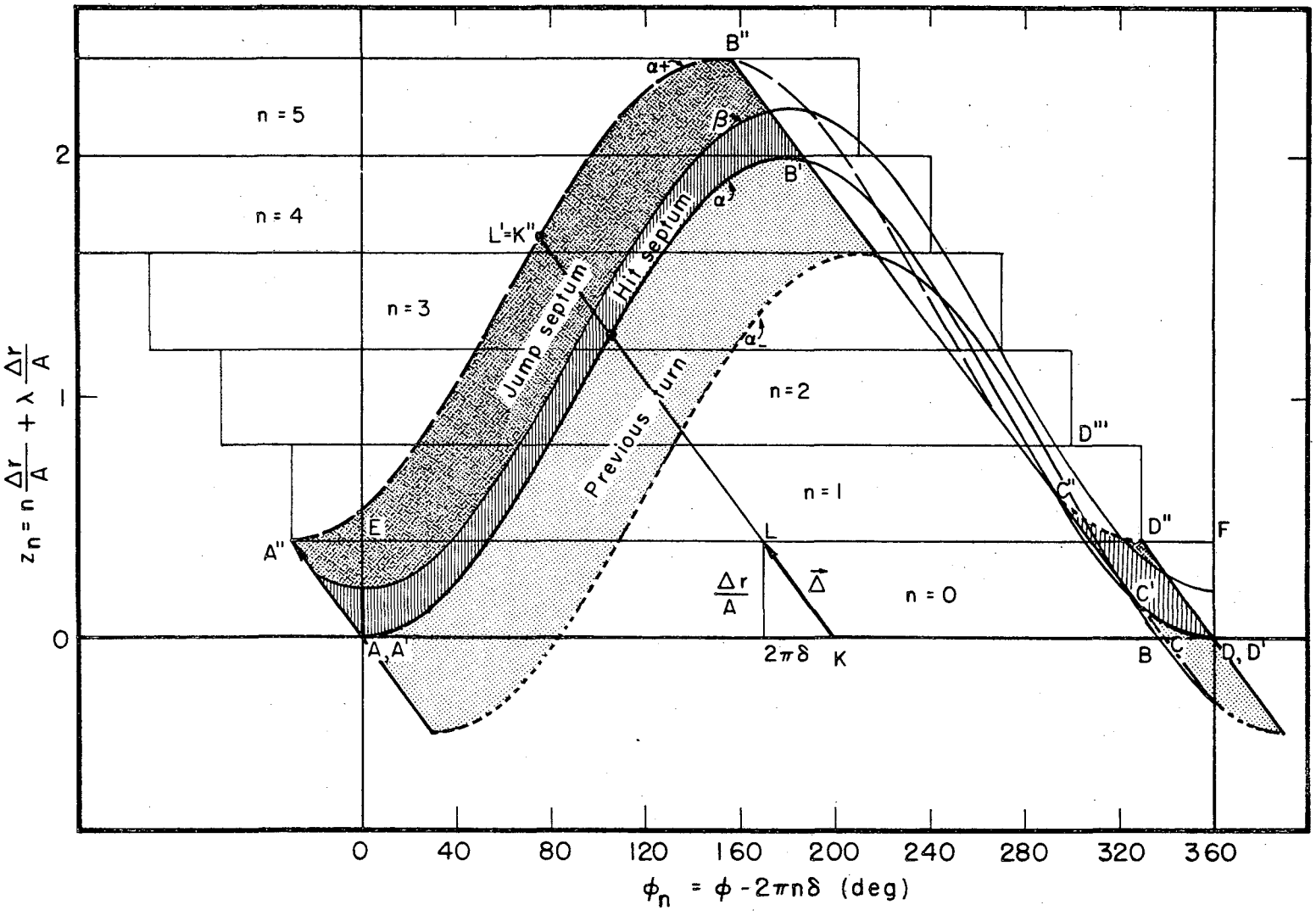

MU-26397

Fig. 4

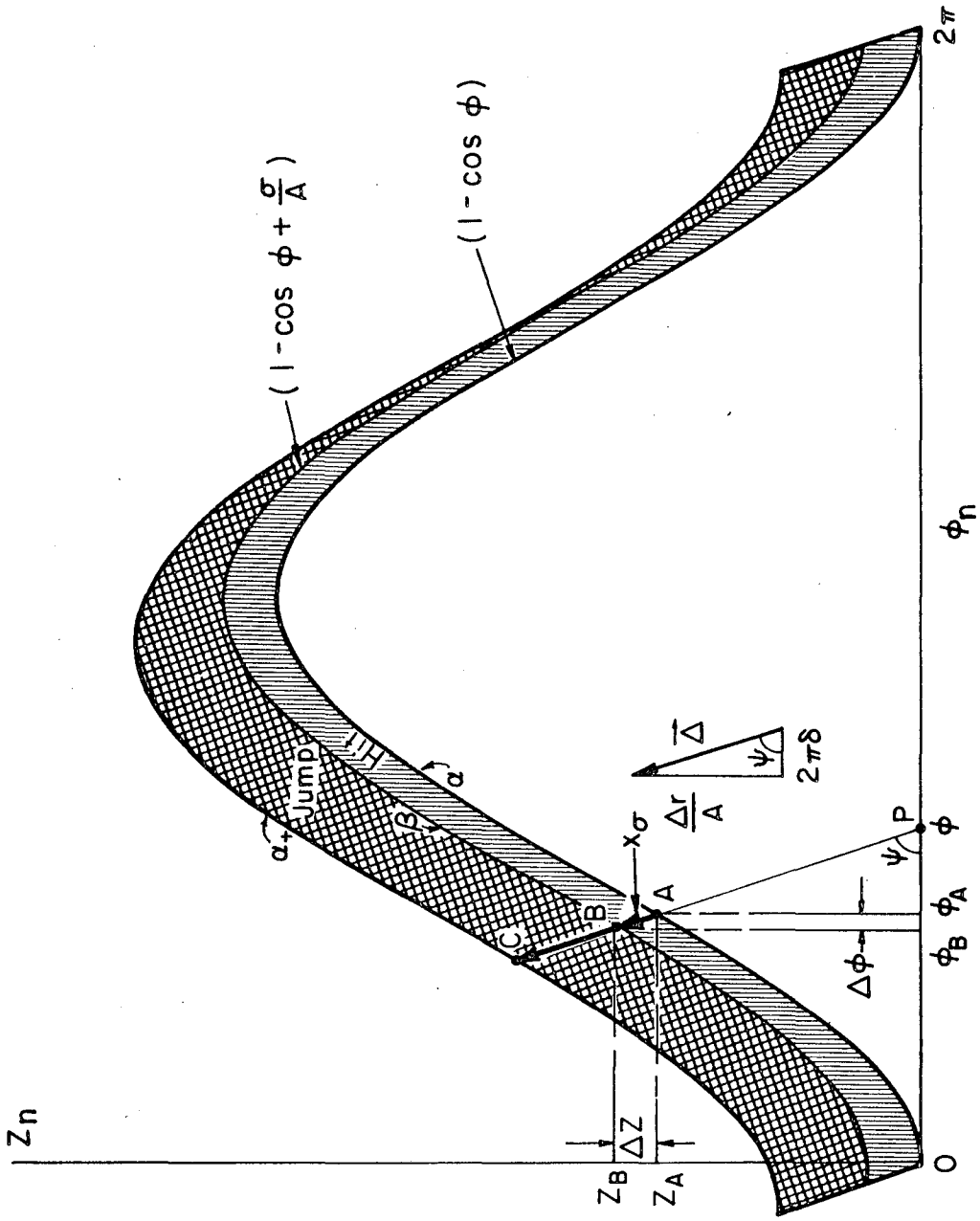

MU-26407

Fig. 5

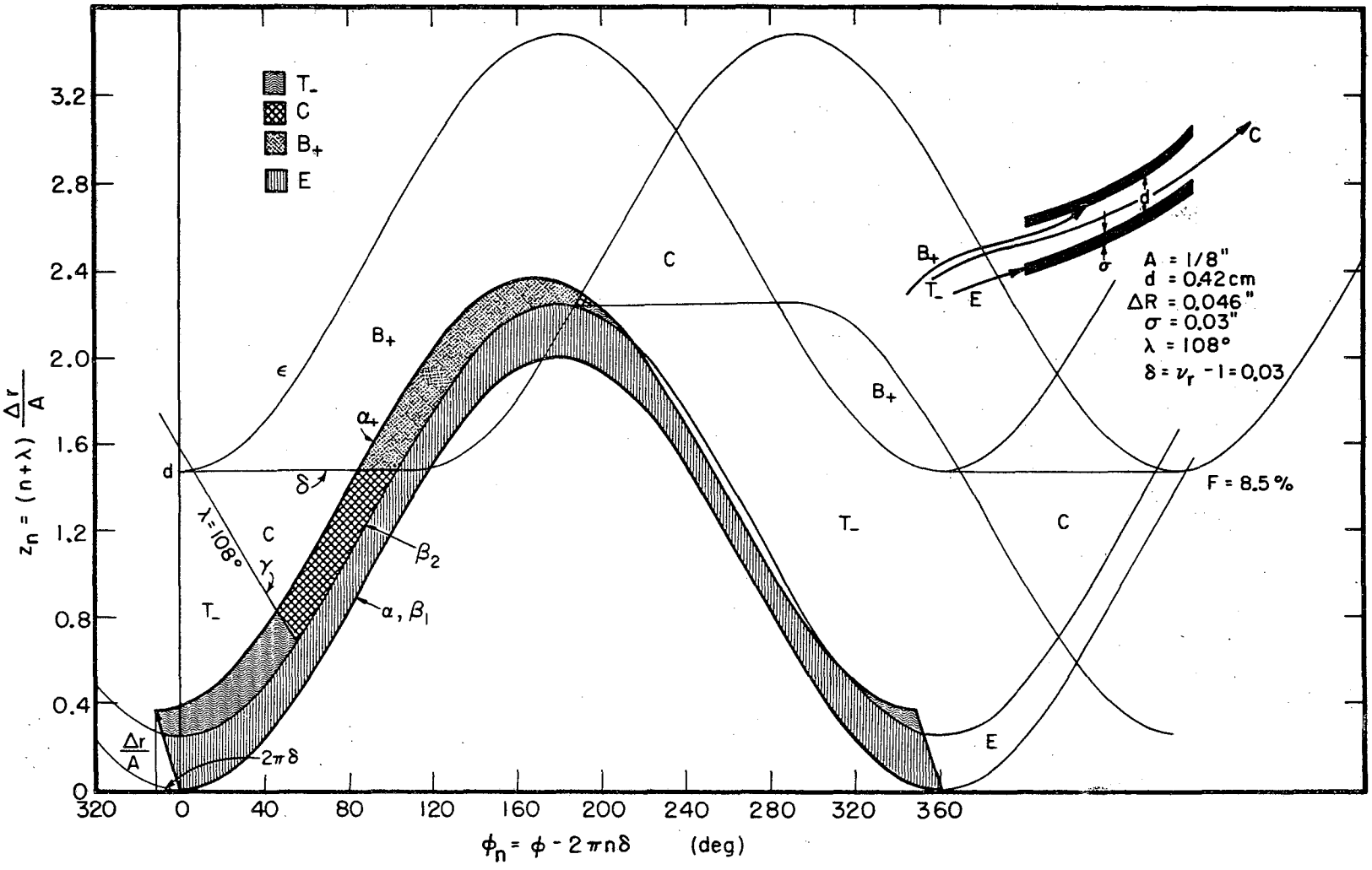

MU-26391

Fig. 6a

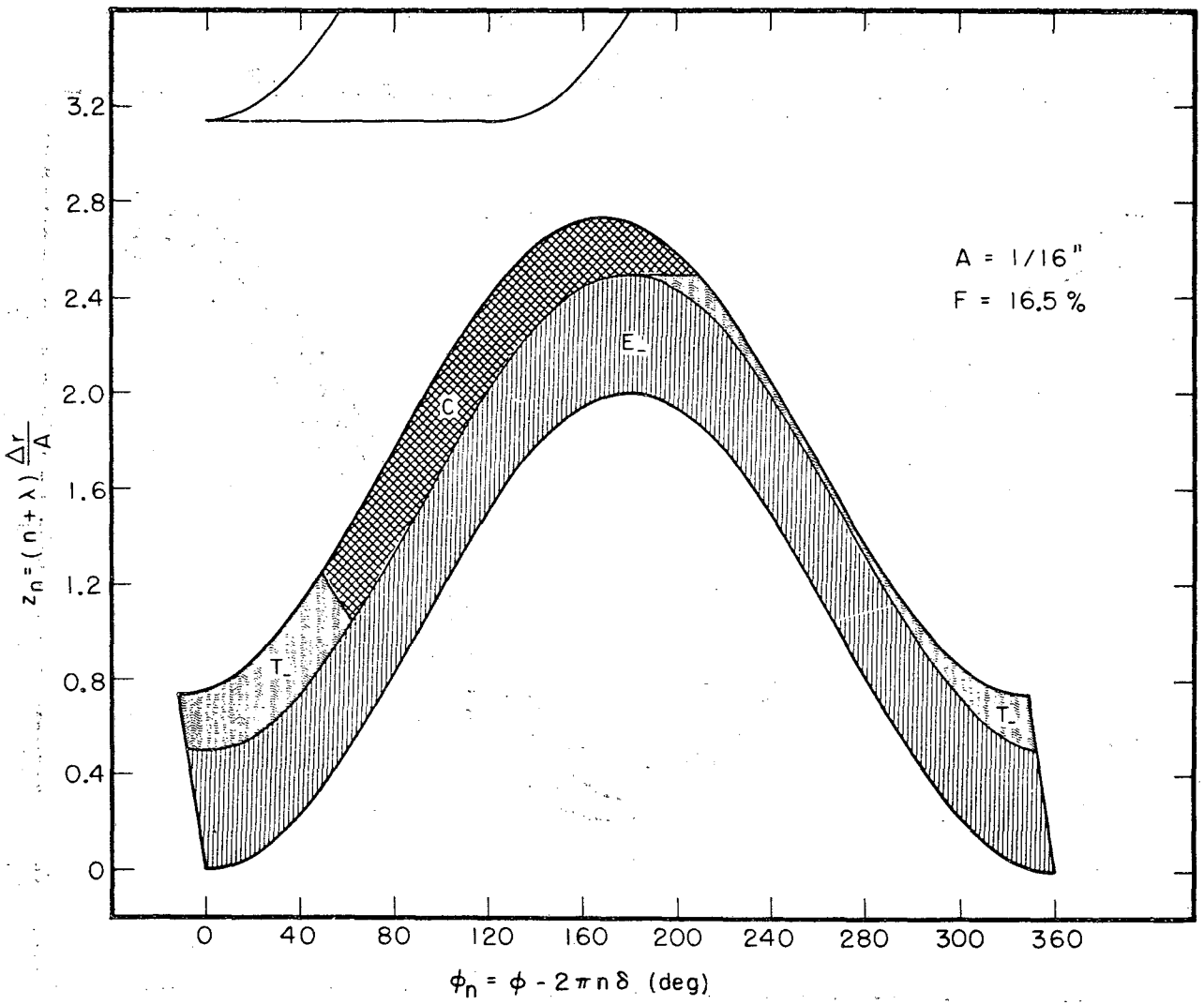
3.2
2.8
2.4
2.0
1.6
1.2
0.8
0.4
0
$z_n = (n + \lambda)\frac{\Delta r}{A}$
A = 1/16"
F = 16.5 %
C
E
T
T
0
40
80
120
160
200
240
280
300
360
$\phi_n = \phi - 2\pi n\delta$ (deg)
MU-26393

Fig. 6b

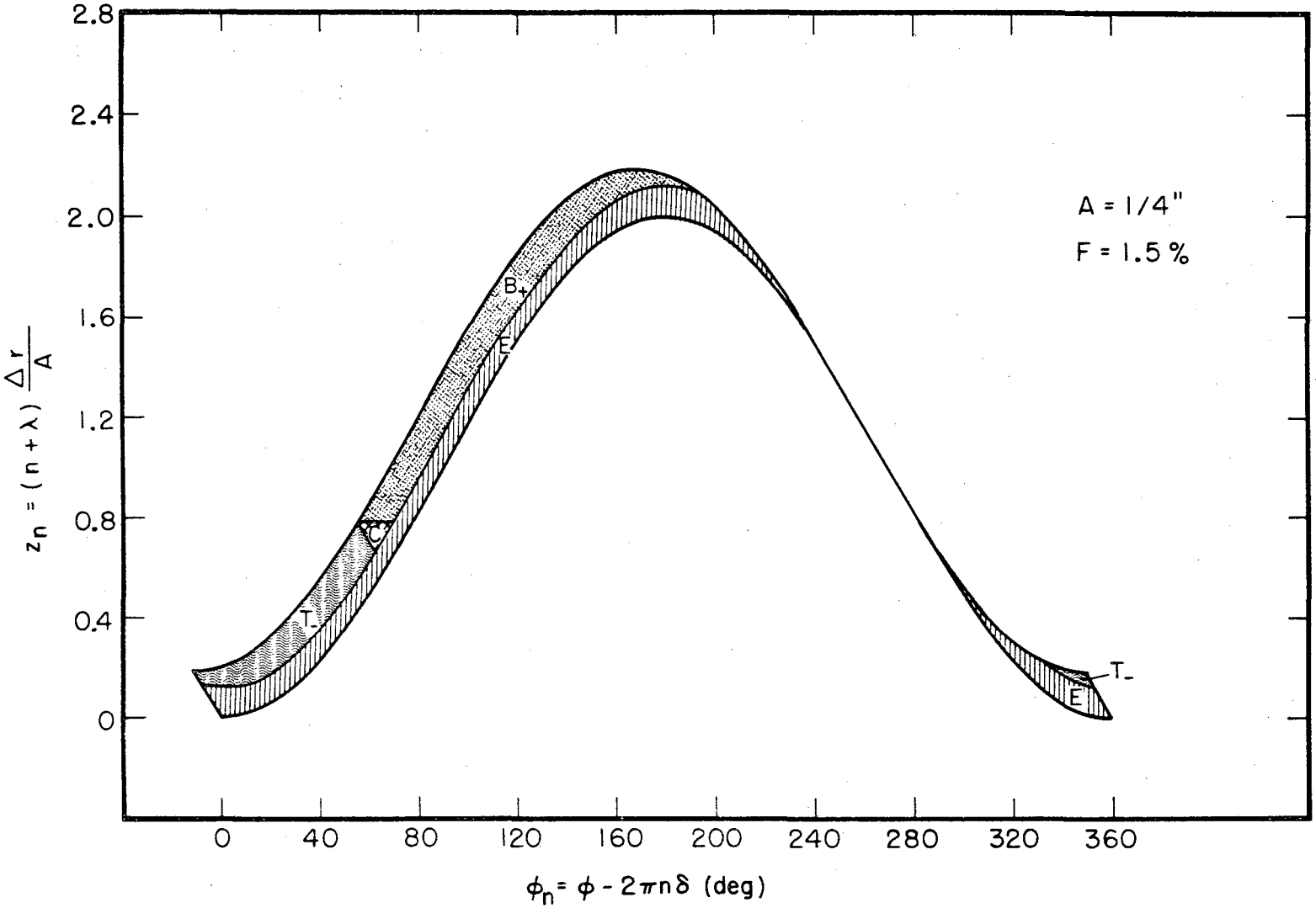

MU-26392

Fig. 6c

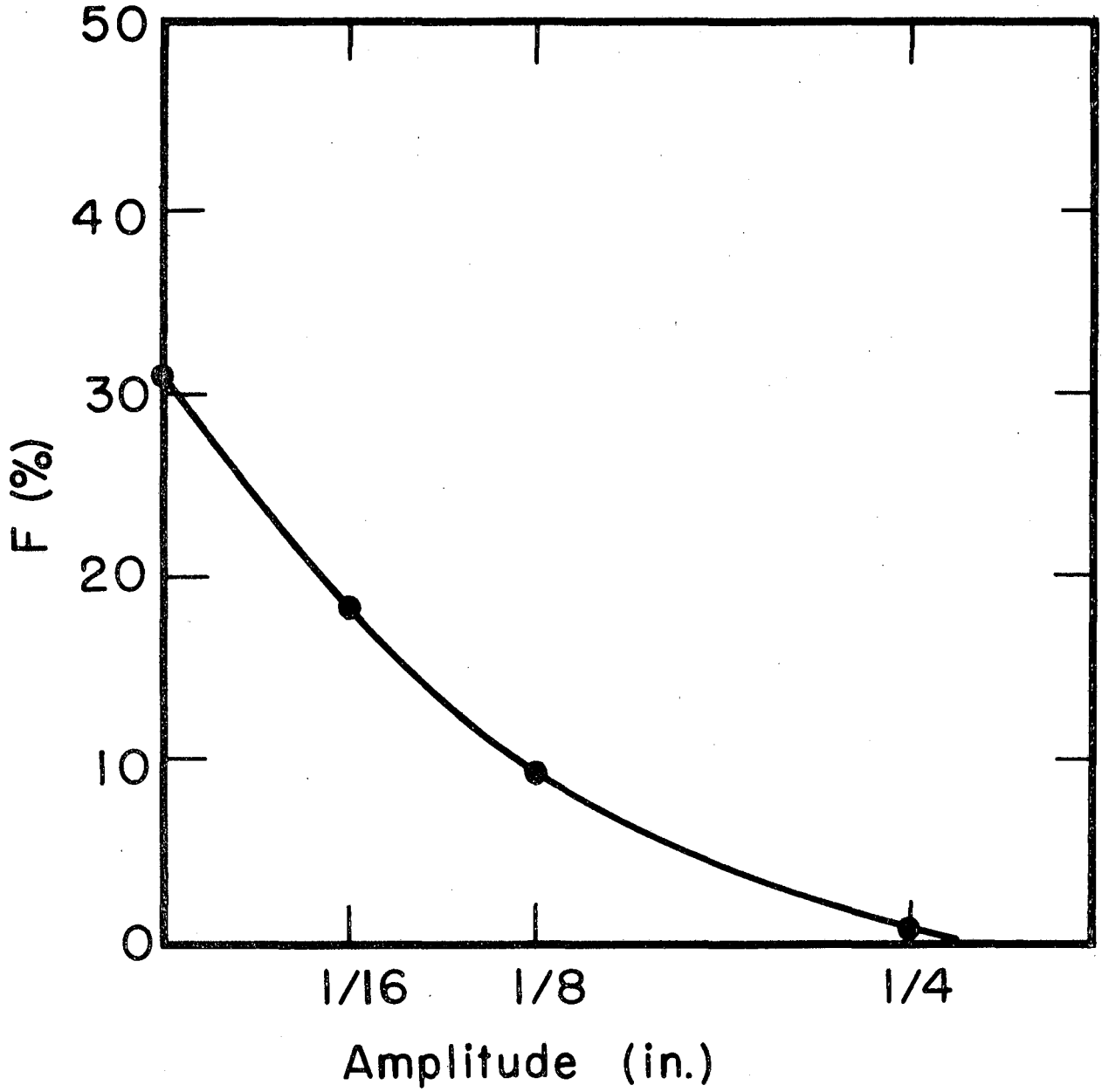

MU-26366
Fig. 6d

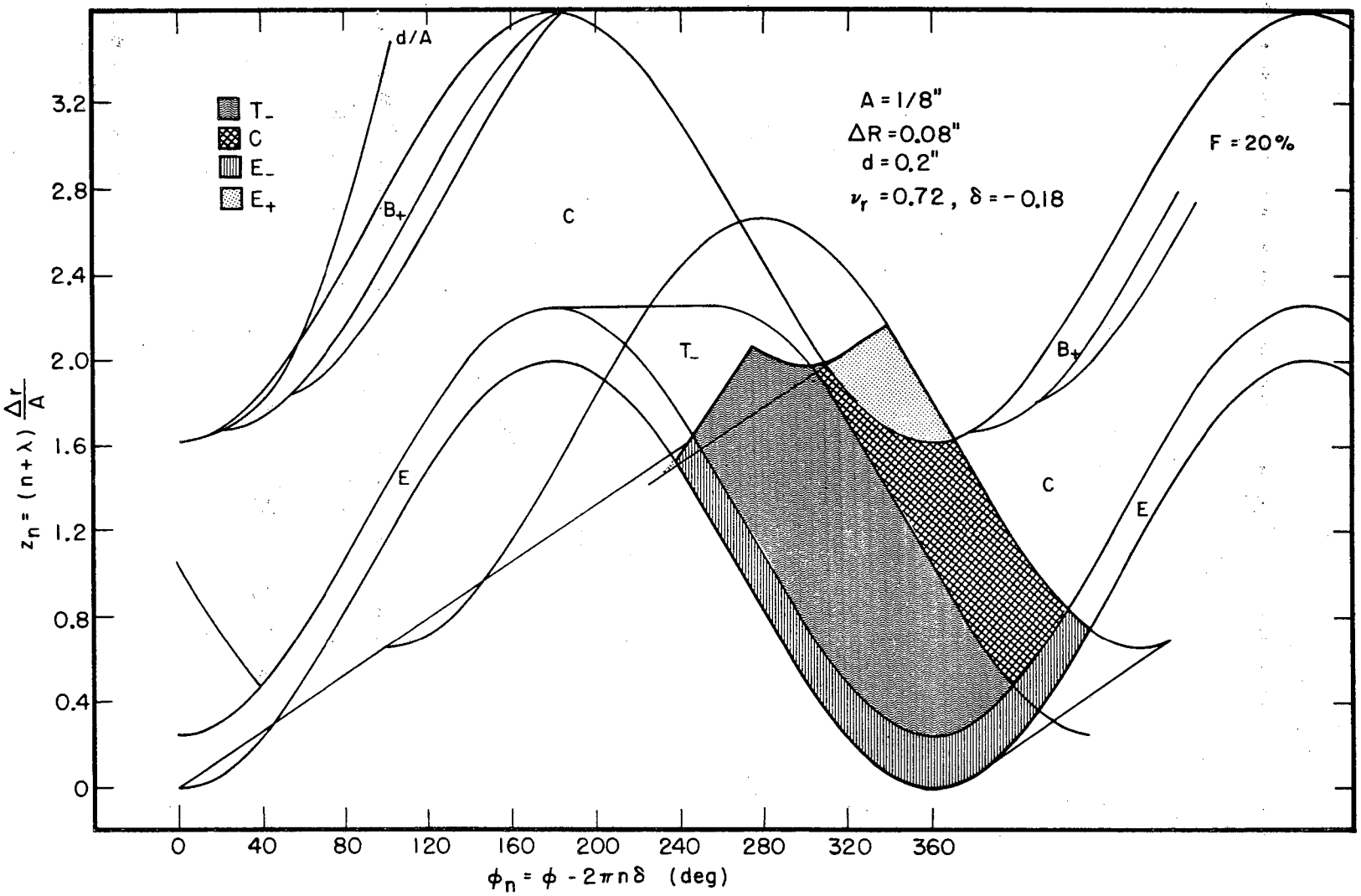

MU-26394

Fig. 7

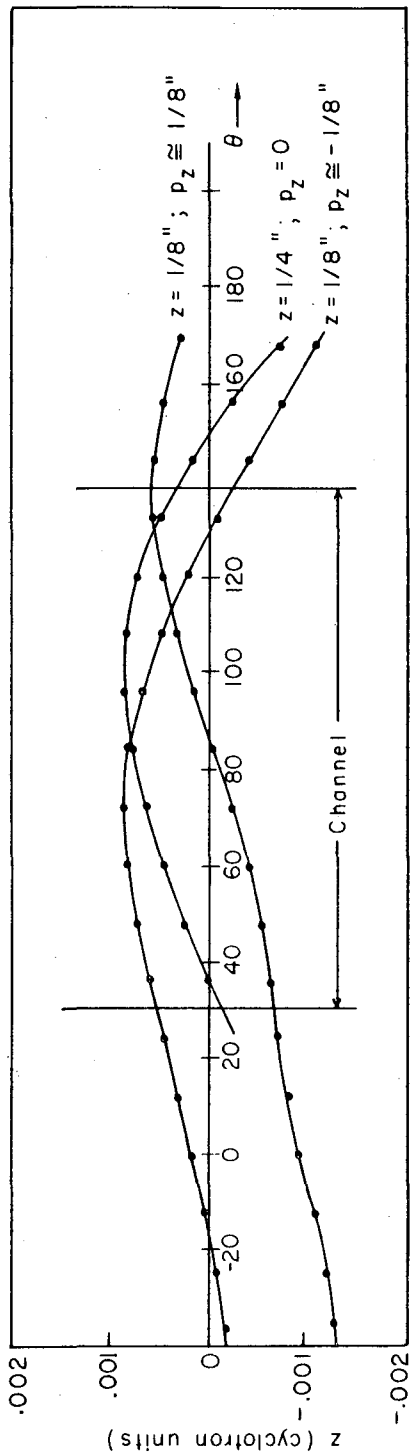

MU-26389

Fig. 8

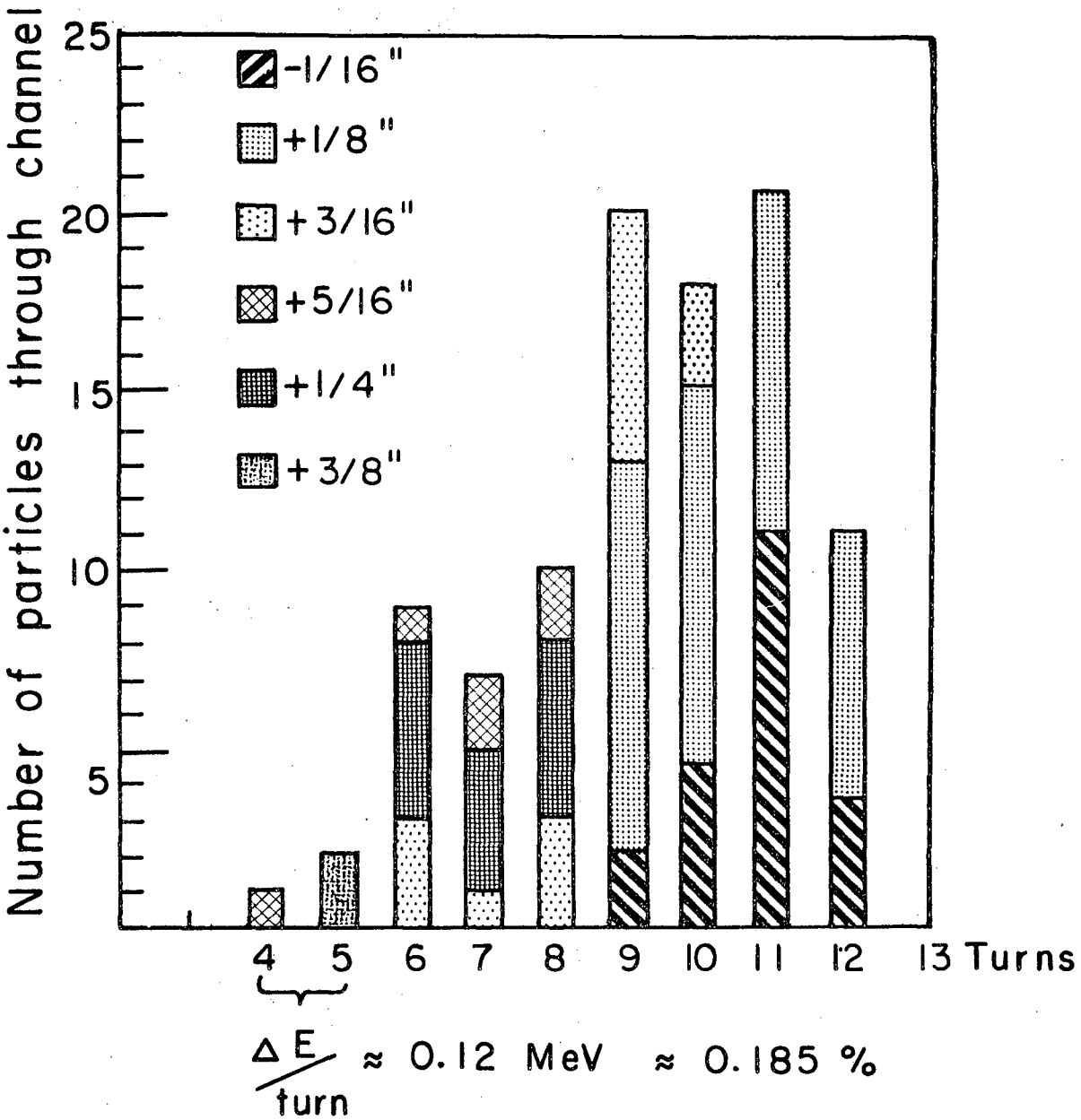

MU-26365

Fig. 9

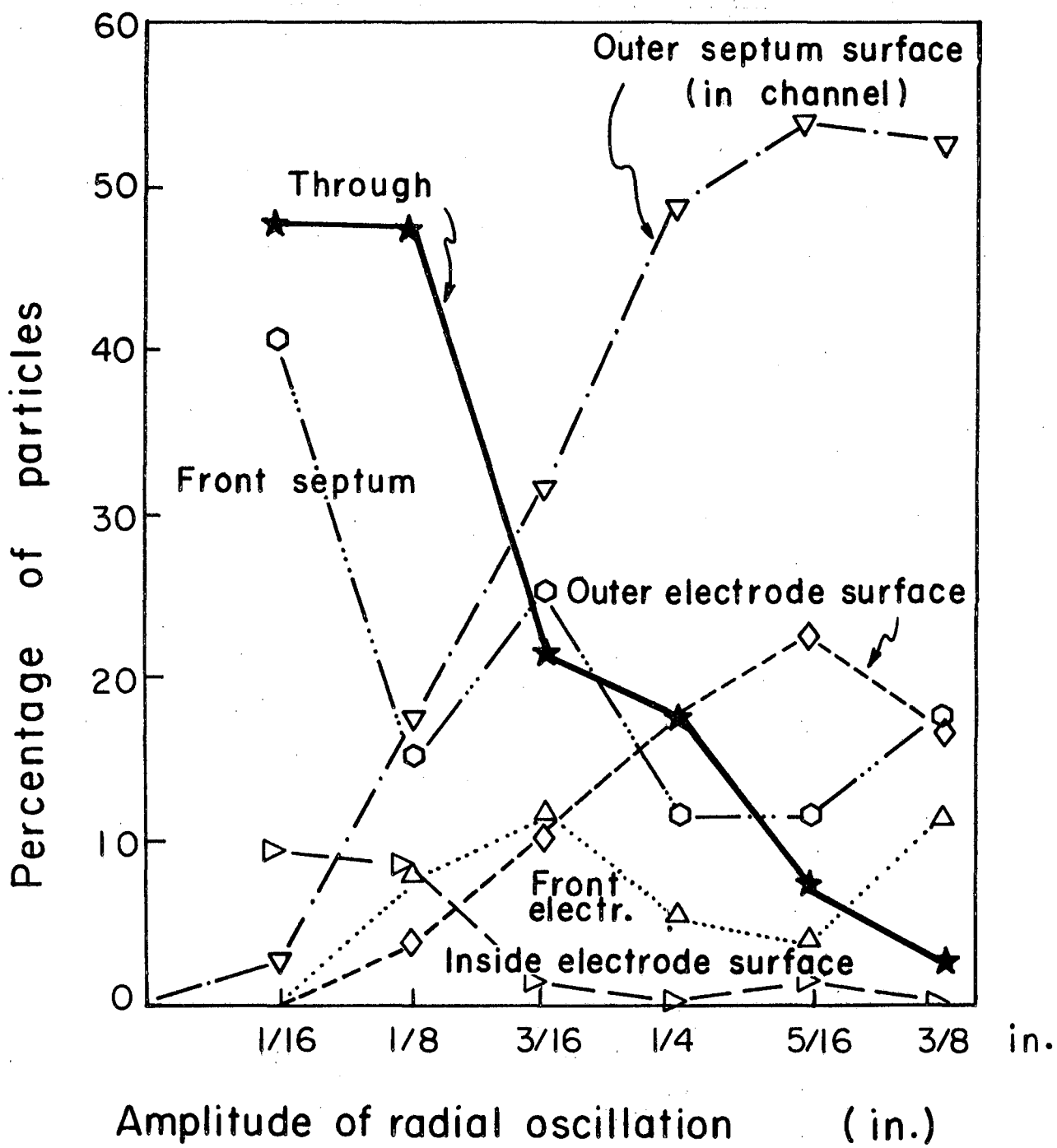

MU-26368
Fig. 10

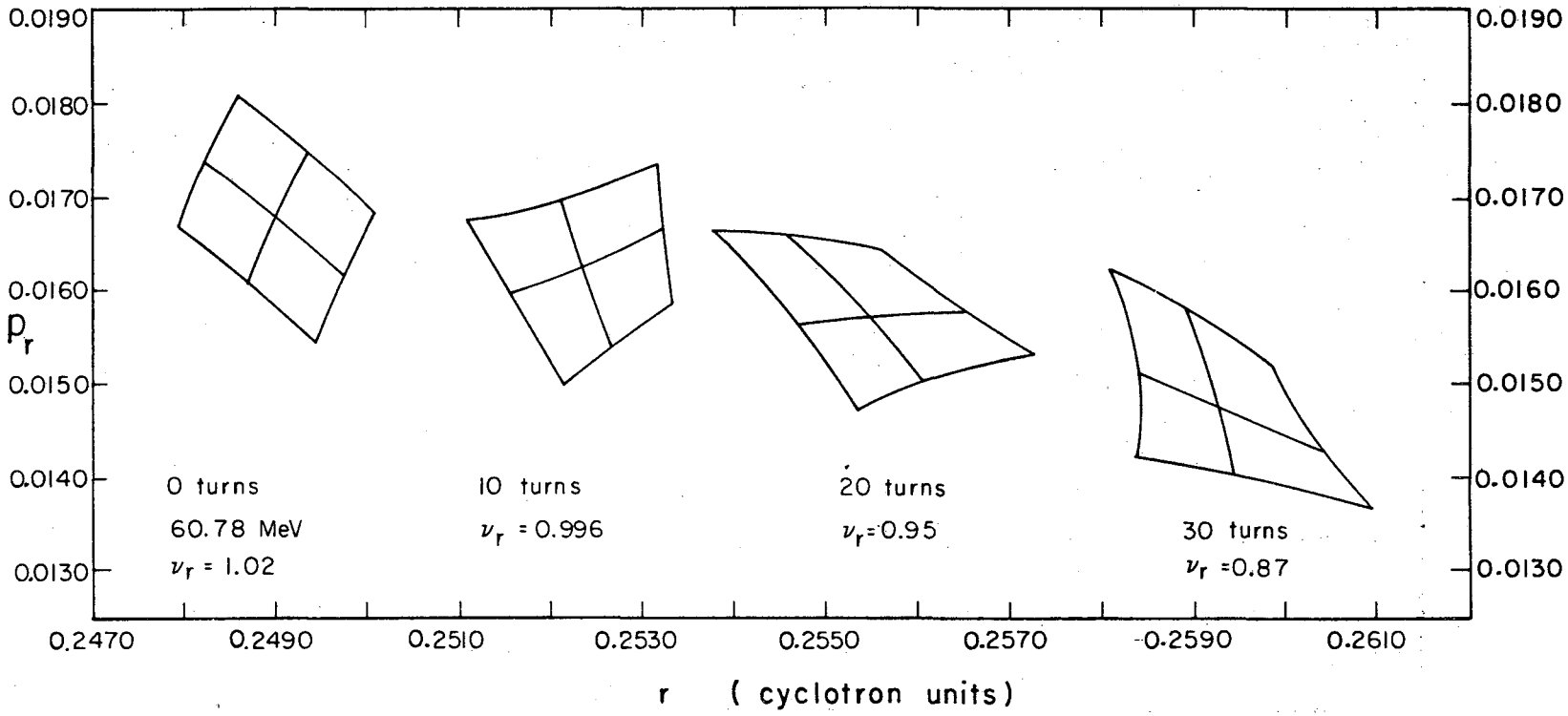

MU-26388

Fig. 11a

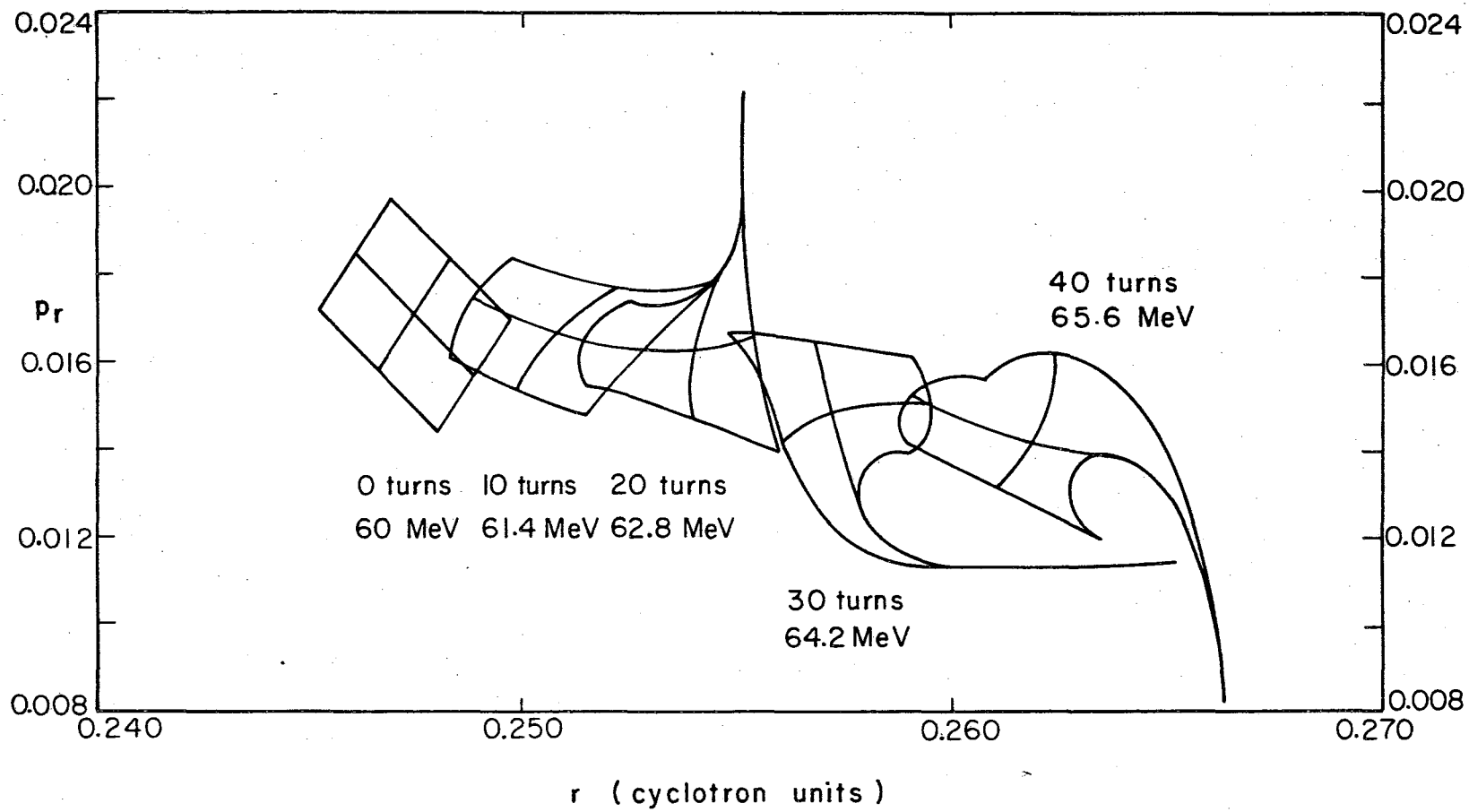

MU-26635
Fig. 11b